NIST-GCR-98-759

Investigation of Droplet Penetrations through Complex Openings of Compartments

S.C. Yao and L.S. Hung
Department of Mechanical Engineering
Carnegie Mellon University
Pittsburgh, PA 15213

United States Department of Commerce
Technology Administration
National Institute of Standards and Technology

NIST-GCR-98-759

Investigation of Droplet Penetrations through Complex Openings of Compartments

Prepared for
U.S. Department of Commerce
National Institute of Standards and Technology
Gaithersburg, MD 20899

By
S. C. Yao and L.S. Hung
Department of Mechanical Engineering
Carnegie Mellon University
Pittsburgh, PA 15213

October 1998
Issued November 1998

Notice

This report was prepared for the Building and Fire Research Laboratory of the National Institute of Standards and Technology under Grant No. 60NANB5D0093. The statement and conclusions contained in this report are those of the authors and do not necessarily reflect the views of the National Institute of Standards and Technology or the Building and Fire Research Laboratory.

Abstract

The use of fine water mist as one of the possible Halon 1301 replacements has been identified for certain fire suppression situations in equipment compartments. One current research effort is to apply the water mist sprays to suppress the fire occurring in hidden location behind obstructions or inside the equipment compartments.

Since the mist usually contains a spectrum of drop sizes, the smaller mist droplets may follow the gas streams closely and penetrate directly through the slots of the obstructions while the larger droplets may be intercepted or impacted by the obstructions. When the mist droplets are approaching the structures, the overall penetrating process of the mist flow through the obstruction depends strongly on the transport of the mist droplets in the gas streams, the ability of the droplets flowing through the obstruction, and the behavior of droplets subsequent to the impaction.

The present research presents an integrated approach to model the penetration of water mist through the obstructions for fire suppression applications. Firstly, numerical investigations employing the two-phase Navier-Stokes equations are achieved using computational fluid dynamics (CFD) to evaluate the overall transport of droplets in the vicinity of the openings, which include rectangular strips and a 3-D screen object. In particular, the motions of the droplets coupled with the gas flow field around the objects are analyzed. The deposition of droplets on the objects and their penetration through the spacing of the objects are also formulated. Then, experimental investigations are performed to address the actual impacting phenomena of droplets on objects. Droplet generators are designed to generate droplets in a variety of operating conditions. Structures such as cylindrical wires and mesh screens are examined in the impaction experiments. Images of the impacting phenomena are analyzed through digital image processing. Non-dimensional regime maps and the correlations of the impaction outcome are also developed. The conclusions from both the numerical and experimental investigations are integrated to provide an overall understanding to the complex interaction phenomena and to establish a procedure for predicting the outcome of similar processes.

Acknowledgment

This research was supported by the United States Department of Commerce, National Institute of Standards and Technology under Grant No. 60NANB5D0093, with Dr. William Grosshandler and Dr. John Yang serving as Scientific Officers.

Table of Contents

List of Figures

Nomenclature

Symbol	Description
d	Diameter of the incoming droplet, [μm]
D	Diameter of the wire of the screen, [mm]
D'	Diameter of the dripping drop, [mm]
D_j	Diameter of the liquid jet, [μm]
D_o	Diameter of the orifice or nozzle, [μm]
D_t	Width of the object or deposition target, [mm]
f	Prescribed frequency of the piezo-electric vibrations, [Hz]
F_{bi}	Body force, [N]
g	Gravitational constant, [m/s^2]
h	Height of the wire screen, [mm]
k	Turbulent kinetic energy, [J]
L	Clear width of mesh opening on screen, [mm]
L_1, L_2	Major and minor axes of the prolate spheroid, [mm]
m_p, M	Mass of a single droplet, [kg]
N	Number of meshes per inch length
r_p	Droplet radius, [μm]
S_Φ	Source terms of gas phase
$S_{\Phi p}$	Source term of dispersed phase
u'	Turbulent fluctuation velocity, [m/s]
U	Gas velocity, [m/s]
v	Droplet velocity for numerical analysis, [m/s]
V_j	Velocity of the liquid jet, [m/s]
V_o	Incoming droplet velocity, [m/s]
V_t	Terminal velocity of the droplets, [m/s]

NON-DIMENSIONAL PARAMETERS

B	Blockage fraction, defined in equation (2.10) (Fraction of the width of blocking object to the width of flow domain)
Bw	Wire Bond number, defined in equation (4.5)
C_D	Drag coefficient
K	Inertial impaction parameter, defined in equation (2.9)
R	Size ratio of wire diameter to the incoming droplet diameter, defined in equation (4.3)
R'	Size ratio of the dripping drop to the wire diameter, defined in equation (4.4)
Ret	Reynolds number based on the width of object = $\rho_p D_t U/\mu$
S	Screen Parameter, defined in equation (5.1)
We	Droplet Weber number, defined in equation (4.1)

GREEK SYMBOLS

α	Penetration efficiency, defined in equation (2.11)
β	Solid fraction of the screen opening
δ	Distance between the centers of the impacting droplet and the wire, [μm]
λ	Stopping distance, defined in equation (2.8), [m]
η	Collection efficiency, defined in equation (2.7)
μ	Viscosity of the surrounding fluid, [Ns/m^2]
ρ_a	Density of the surrounding fluid, [kg/m^3]
ρ_p	Density of the droplet, [kg/m^3]
σ	Surface tension of water, [N/m]
τ	Droplet relaxation time, [s]
Δ	Offset ratio of droplet relative to wire, defined in equation (4.2)
Γ	Effective viscosity

Chapter One

Introduction

1.1 General Background

The abolition of fire suppressant Halon 1301 under the Montreal Protocol has led to the research and development on the use of fine water mist as one of the possible Halon replacements in certain fire suppression applications. The use of fine water mist for certain fire suppression applications has been discussed by Jones and Nolan (1995) and by Ramsden (1996). One current on-going research effort is to apply the water mist sprays to suppress fire occurring inside equipment compartments. However, the penetration of water mist is a very complex phenomenon. Whether the mist spray can reach the fire inside the equipment compartment or not is strongly dependent upon the transport of mist droplets in the gas streams, the ability of the droplets penetrating through the openings of the compartment, and the behavior of droplets subsequent to the penetration.

The fine water mist normally contains a spectrum of droplets with diameters ranging from 10 μm to 200 μm (Lefebvre, 1989) while the drops of the typical water sprinklers have spectrum usually larger than 250 μm (Jones and Nolan, 1995). However, the use of mist sprays verses sprinkler drops in certain fire situations is very much dependent upon how the water drops reach the fire location. For example, for the fire occurring in an open space, larger droplets from water sprinklers, with greater momentum, may be able to penetrate the plume to the fire while smaller mist droplets may be pulled into the fire from the side by the strong gas convective streams induced by the fire source. Furthermore, if the fire occurs in hidden locations behind certain obstructions in an equipment room or in a computer and electrical compartment, fine water mist may be superior because it has a better capability to circulate around the obstructions by closely following the air streams and to penetrate into the compartment through the opening slots.

In addition, for the water mist droplets which are intercepted by the structures, the intercepting process of the droplets is influenced by the configurations of the opening which could be bars, slots, and screens. At present, there is not much published literature about the interaction between the mist droplets and these opening structures.

Although the phenomena are complex, the interactions generally include the transport of droplets around the impacted objects, and the impaction and deposition of droplets on the surface of the objects. Once these principal phenomena are properly understood, a comprehensive understanding of the overall process can be integrated. This is the main focus of the current investigation.

The interaction of the water mist and the opening structure of compartment has been modeled through numerical computations and experimental investigations. The objective is to reveal the transport mechanisms, impaction, and penetration of water mist droplets, and to predict their implications through compartment openings during fire situations (Hung and Yao, 1996a, 1996b, 1997).

In many actual situations, there may exist high temperature gradient regions and the water mist may be vaporized rapidly. However, this present study concentrates mainly on the impacting dynamics and transport of water mist droplets in an isothermal environment. Therefore, the model of droplet evaporation is not accounted for in this study. With the consideration of droplet evaporation, the larger mist droplets might evaporate and gradually become smaller while smaller droplets might disappear very soon. Therefore, the spectrum of the water mist may become more complex and there may exist some optimal mist conditions which could be effective for certain fire suppression situations.

1.2 Transport of Water Mist for Fire Suppression

The overall transport process of the water mist droplets is strongly influenced by the flow condition as well as by the structural shapes of the obstructions or openings. The smaller in-flight droplets with tens of micron in diameter may follow the air stream closely with better penetrating capability while the larger ones may be intercepted or impacted by the structures.

When the droplets flow along with the gas streams, the primary transport mechanism of the droplets is basically an inertial-controlled aerodynamic process. The dynamics of the droplets are coupled with the motion of the gas streams. In the vicinity of the object, the gas streams will bend away from the object (stagnation point flow), and the droplets might follow the gas streamlines until they begin to curve around the object. The larger droplets, with higher inertia, may continue their motion toward the object and impact upon its surface. On the other hand, the smaller ones may follow the gas streams closely to flow around the object without hitting it. This process is commonly known as the inertial impaction.

The inertial impaction of particles on objects such as cylinders, spheres, disks, and rectangular strips has been examined carefully by various researchers both theoretically (Langmuir and Blodgett, 1946; Ranz and Wong, 1952; Golovin and Putman, 1962; Noll and Pilat, 1970; and Konstandopoulos et al., 1993) and experimentally (May and Clifford, 1967; Noll and Pilat, 1970; Eleftheriadis and Colbeck, 1992; and Hahner et al., 1994) for aerosol research. Among these works, the common interests were to analyze the impaction characteristics and its corresponding collection efficiency on the objects.

If the droplets are flowing uniformly across the flow domain from upstream towards a single object or a group of objects, some droplets may impact and be retained on the surfaces (deposition) while others may be able to escape through the spacing between the objects and continue to move on with the gas streams further downstream (penetration). The governing factors of this transport situation are the flow condition of the gas streams, the properties of the droplet, and the geometry of the objects. While it is apparent that both mechanisms, deposition and penetration, are closely connected, there is no information available from the published studies addressing this issue. Therefore, it is desired to explore and to devise a methodology to evaluate the penetration of droplets through the spacing between the objects.

In addition to the above upstream droplet transport phenomena, it is also known that a cross flow over an object or a bluff body would induce secondary flow and transient vortex structures downstream behind the body at a certain range of flow conditions, primarily distinguished by the Reynolds number. Therefore, for those droplets co-flowing with the gas streams and penetrating through the gaps between the objects, their trajectories might be

strongly influenced by the nature of wake behind the objects which can usually be characterized by the alternate vortex shedding. However, it has not been revealed from the available literature of how the wake and the time dependent vortex shedding structure would affect the motions and trajectories of the droplets.

Therefore, at many occasions, the water mist may behave very differently during transport and shows advantages or specific drawbacks than the conventional water sprinkler drops. There are three typical situations studied in this research study.

First, due to the drag force exerted by the surrounding air, the falling droplets with different sizes exhibit different terminal velocities. Figure 1.1A shows that when the mist is injected to an open fire, the mist droplets might penetrate into the fire from top or from the side. Smaller droplets may have a better chance to be pulled into the fire by the suction effect from the side, and the volumetric spectrum of the droplets will be very critical to this suction process. In addition, the traveling time of the mist droplets could be longer than that of the sprinkler drops.

Secondly, as shown in Fig. 1.1B, if the water mist is used to suppress a fire which occurs behind a structure or an obstruction, whether the mist can circulate around the obstruction to reach the fire behind it will also be a critical concern.

Finally, the opening structure of a typical compartment usually consists of discrete partitions such as slots and strips (Fig. 1.1C). Since the existence of these structures may reduce the penetrating effectiveness of the mist into the compartment by blocking its entry, it is important to estimate the fraction of the total mist which would penetrate into the compartment through these opening structures.

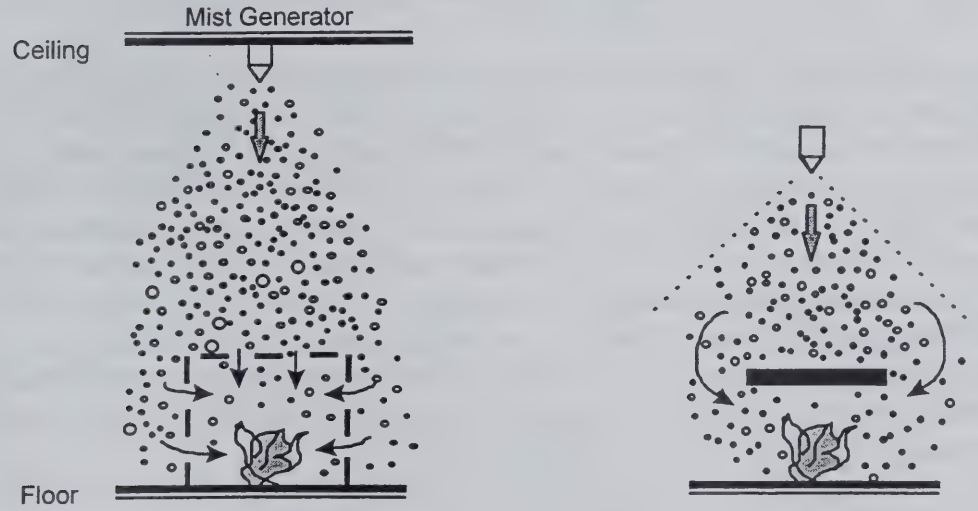

A B

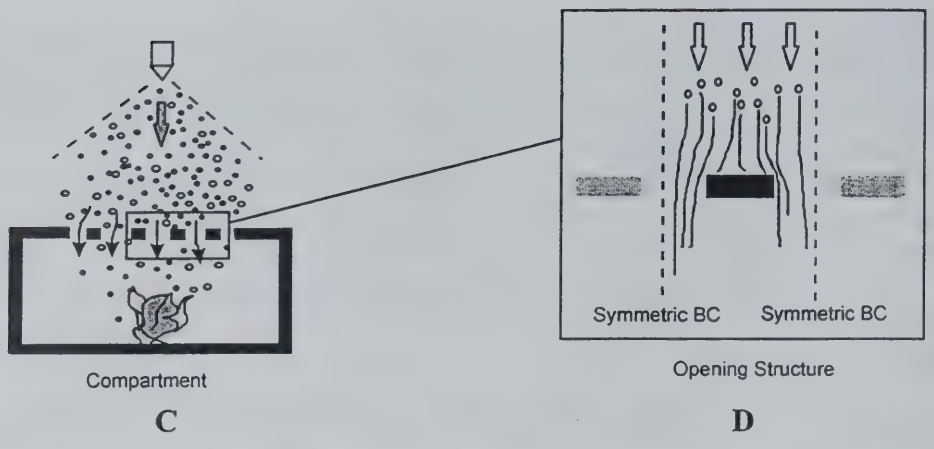

Figure 1.1 Some phenomena of fire situations

A. Mist penetrates into an open fire
B. Mist penetrates around an obstruction
C. Mist penetrates into a compartment through the opening slots
D. Enlarged view of droplets penetrating through the compartment openings

1.3 Impaction of Mist Droplets on Compartment Openings

As in continuation with the previous discussion, the penetrating process of the mist flow into an equipment compartment through the openings is very complex. While the smaller droplets in the mist may follow the air stream closely and penetrate directly through the slots of the openings, the larger ones may be intercepted or impacted directly by the opening structures. Figure 1.2 displays the phenomena of mist droplets penetrating into the compartment. However, part of the mist which is intercepted by the structures may build up liquid films and subsequently penetrates into the compartment in the form of larger drop sizes from the detachment of liquid films. Since the intercepting and impacting processes are strongly influenced by the shapes of the openings which could be bars, ventilating screens, or multiple slots, it is important to understand the interaction between the water mist droplets and the opening structures.

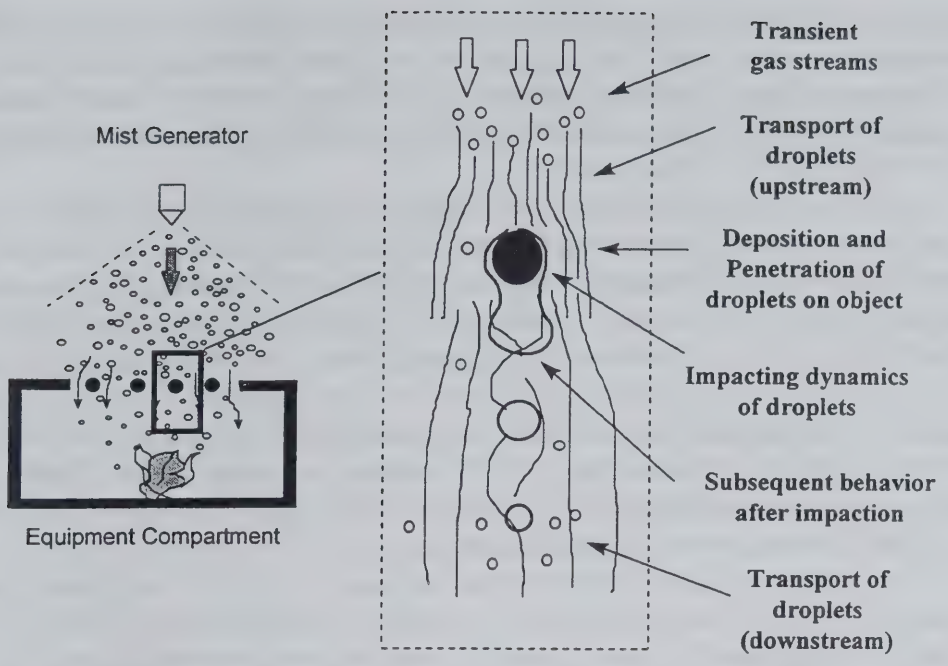

Figure 1.2 A schematic of mist penetrating and intercepting on an opening structure

The impaction process of droplets on surfaces involves a number of complex mechanisms. Therefore, comprehensive research effort has been focused on revealing the fundamental behavior of droplets impacting on solid surfaces.

Among the extensive amount of published studies, research works have been performed on the impacting phenomena of droplets onto large planar solid surfaces (Harlow and Shannon, 1967; Lesser, 1980; Cazabat, 1987; Yao and Cai, 1988; Chandra and Avedisian, 1991; Cohen, 1991; Kral et al., 1993; Fukai, et al., 1995; and Zhao et al. 1996a, 1996b). Various approaches such as sequential photographic technique, high speed photography, digital imaging analysis, numerical computation, and analytical modeling have been undertaken to study the spreading behavior, the contact angle, the angle of impact, the wetting effect, the breakup and disintegration, the deformation profile, and the fluid dynamics of the impacting droplets. A comprehensive review by Rein (1993) presented the phenomena of liquid drops impacting on both solid and liquid surfaces. He concluded that the outcome of droplets impaction depends on the properties of the droplet, the droplet impact velocity, the condition of the impacted surface, and the ambient fluid. The impacting phenomena could include a combination of bouncing, spreading, splashing, and coalescence.

In many other situations, however, the geometry of the impacted surface may be very complex and far from being planar. For example, in the agricultural applications, sprays of pesticide and herbicide are targeted to cover the plants such as crops, leaves, and stems, all with very complex geometric shapes and sizes. In the medical field, nasal sprays have been used extensively. Drops of medication are expected to deposit onto the surface on the lung directly. However, the trajectories of the in-flight droplets might be intercepted by the nasal hair in the nostrils and bronchial tubes before even reaching the desired locations in the lung. Hair sprays are also a specific example: Hair size is typically on the order of 50 to 80 μm

which is very compatible with the size of the fine mist sprays. There is a tremendous need to understand how hair spray droplets interact with the hair texture of comparable size. When the droplets collide with these surfaces, the spreading and the splashing characteristics would be quite different and the results of droplets impacting on planar surfaces may not be directly applicable to the non-planar cases.

In contrast, very limited published literature is available on droplets impacting on non-planar surfaces. An early study by Levin and Hobbs (1971) used a high speed camera to examine the droplets impacting on a curved wall with the radius of curvature much larger than that of the droplet. Later, Dear and Field (1988) also investigated the surface geometry effect in liquid/solid impact using high speed photography to study the propagation of shock waves in both the liquid and the impacted medium. More recently, Bussmann et al. (1997) studied the phenomena of a single 2 mm water droplet impacting on an arbitrary surface geometry such as a 45 degree inclined flat surface and a sharp edge. They suggested that the phenomena of droplets impacting on these arbitrary surfaces were very different than that of the typical flat surface impacting situation.

In the above published studies, the droplets are usually very small compared to the dimension of the impacted surface. Very little information has been reported on droplets hitting on surfaces with finite dimensions which are comparable to the sizes of the droplets. A relevant work in this area was performed by Yao et al. (1988). They studied the phenomena of droplets impacting on thin rectangular strips which were heated beyond the Leidenfrost temperature. They showed that when the droplet diameter and the strip thickness were comparable, the impacting phenomena included a combination of splashing and cutting. Recently, Liu et al. (1994) performed a numerical study to examine the spreading behavior and consolidation of molten droplets impinging on a waved target surface. They concluded that when the droplet impacted on a waved surface, it spread in a radially outward direction and maintained a relatively good contact and adhesion with the waved surface. Through these preliminary studies, it is expected that the geometry and size of the impacted surface would play a significant role in the outcome of the droplet impacting phenomena.

1.4 Objectives of the Current Work

This research has been carefully designed to address the key fundamentals of the transport and the impacting dynamics of spray droplets penetrating through the complex openings of compartments. The primary objectives are:

1) To examine numerically the transport of spray droplets around the opening of the compartments. This includes the analysis of droplet motion at the upstream, around, and downstream locations of the objects. In addition, the impaction characteristics and its corresponding collection efficiency and penetration efficiency are also explored.
2) To reveal experimentally the direct impacting dynamics of droplets on to a selection of objects with complex geometry. The designs of two droplet generators which would produce droplets in a variety of operating conditions are explored. Non-

dimensional parameters and regime maps are utilized to identify the impaction characteristics and outcome.

3) To integrate the results together in order to provide a comprehensive understanding and physical insights to the overall transport and impacting dynamics phenomena.

Chapter Two presents the numerical modeling of the transport of spray droplets around the complex objects. Computational Fluid Dynamics (CFD) approach employing a two-phase Eulerian-Lagrangian formulation is used to analyze the transport of both the gas phase and droplet phase around the objects. Formulations are also developed analytically to account for the collection and penetration characteristics of droplets associated with the objects.

The overall experimental apparatus and the procedure are documented in Chapter Three. The theory of producing mono-size droplets will be discussed. The designs of the two mono-size droplet generators, which are capable of generating the droplets in a variety of operating conditions, are also presented. The experimental conditions which cover a wide range of droplet sizes and impacting velocity are described in details.

The experimental study of droplets impaction are presented in the following two chapters. In Chapter Four, the impaction studies on horizontal wires are detailed. Non-dimensional regime maps and correlations are developed to characterize the impacting phenomena. Then, in Chapter Five, the experimental works are extended to the situation of droplets impacting on horizontal wire screens.

In Chapter Six, the contributions of the research are summarized and some potential research areas for further investigation are identified.

Chapter Two

Numerical Investigations of The Transport of Droplets Around Complex Objects

Summary

The transport of spray droplets around the objects is numerically investigated in this chapter. A computational fluid dynamics (CFD) approach is employed to evaluate the two-phase transport in the vicinity of the objects. The transport, impaction, and penetration of droplets over a rectangular strip, a local screen structure, and a group of staggered objects will be illustrated. The purpose of this study is to understand the mechanisms of penetration and impaction of droplets onto the objects. The results from these investigations provide the physical insights for applications such as the water mist penetration and transport for fire suppression and droplets flow over a screen structure.

2.1 Model Formulations

The basic formulations and the computational procedure to solve the set of transport equations for both the gas phase and the droplet phase are presented in the following sections:

2.1.1 Motion of Droplets During Free Falling

This section presents a numerical analysis of free falling droplets. The effect of time delay and change of volumetric spectrum of free falling mist droplets in stagnant air are examined. It is important to understand how the time delay and change of droplet spectrum would affect the deposition flux penetrating into the location at a certain distance from injection.

Assuming a low subsonic speed where the wave drag is negligible, the equation of motion of a single free falling droplet can be represented by the formulation below (Chow, 1979):

$$m_p \frac{dV}{dt} = m_p g - m_a g - \frac{1}{2} m_a \frac{dV}{dt} - \frac{1}{2} \rho_a V|V| \frac{\pi}{4} D_p^2 C_d \qquad (2.1)$$

The terms on the right hand side are the weight, buoyant force, force on an accelerating body (work against the stagnant fluid suddenly set into motion), and drag force by the viscous effect of the surrounding fluid, respectively. The C_d is the drag coefficient which is related to the Reynolds Number based on the drop diameter, given by Chow (1979), with the following correlations:

$$C_d = \begin{cases} \dfrac{24}{\mathrm{Re}} & \mathrm{Re} \le 1 \\ \dfrac{24}{\mathrm{Re}^{0.646}} & 1 < \mathrm{Re} \le 400 \\ 0.5 & 400 < \mathrm{Re} \le 3 \times 10^5 \\ 0.000366\,\mathrm{Re}^{0.5275} & 3 \times 10^5 < \mathrm{Re} \le 2 \times 10^6 \\ 0.18 & 2 \times 10^6 < \mathrm{Re} \end{cases} \qquad (2.2)$$

When the droplet achieves the terminal state, i.e., the d/dt terms in equation (2.1) vanish, the terminal velocity can be found as:

$$V_t = \left[\frac{4g(\rho_p - \rho_a)D_p}{3\rho_a C_d} \right]^{\frac{1}{2}} \qquad (2.3)$$

Equation (2.1) is an ordinary differential equation and it can be integrated numerically using the 4th order Runge-Kutta method to obtain the displacement and velocity as a function of time and droplet size.

The terminal velocity is plotted against the droplet size in Fig. 2.1, and it is proportional to the square root of the droplet size. Higher terminal velocity corresponds to a larger droplet size. Figure 2.2 shows the displacement of the droplets as a function of droplet size and time. It is worth noted that the typical time of travel for the mist spectrum is on the order of seconds, much longer than that of the larger drops. Typical time of travel (or delay) for the mist sprays of 70 μm to arrive a distance of 2 m would take about 16 seconds.

If the initial drop size distribution can be represented using a Rosin-Rammler equation (Fig. 2.3), the volumetric number density distribution of droplet can be obtained by dividing the Rosin-Rammler droplet distribution by the terminal velocity for each droplet size. The minimum drop size used to determine the distribution is 5 μm. As shown in Fig. 2.4, the volumetric distribution curve is highly skewed to the left, indicating that there are more smaller droplets present than the larger droplets. This indicates how much in proportion of droplets with different sizes might be present at a specific location in the flow domain.

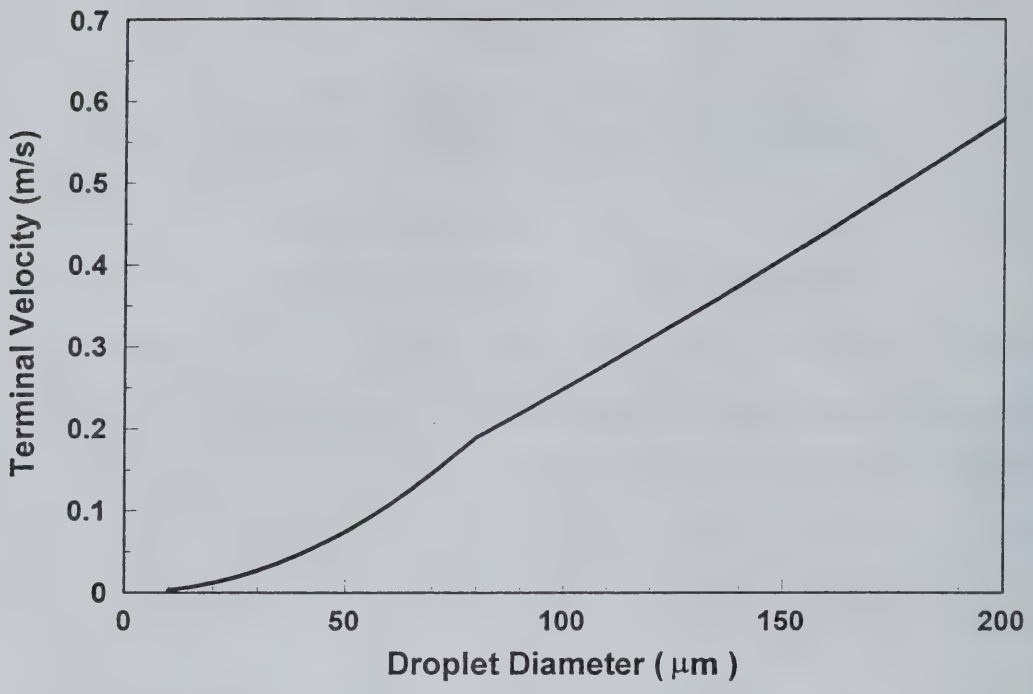

Figure 2.1 Terminal velocity of mist droplets

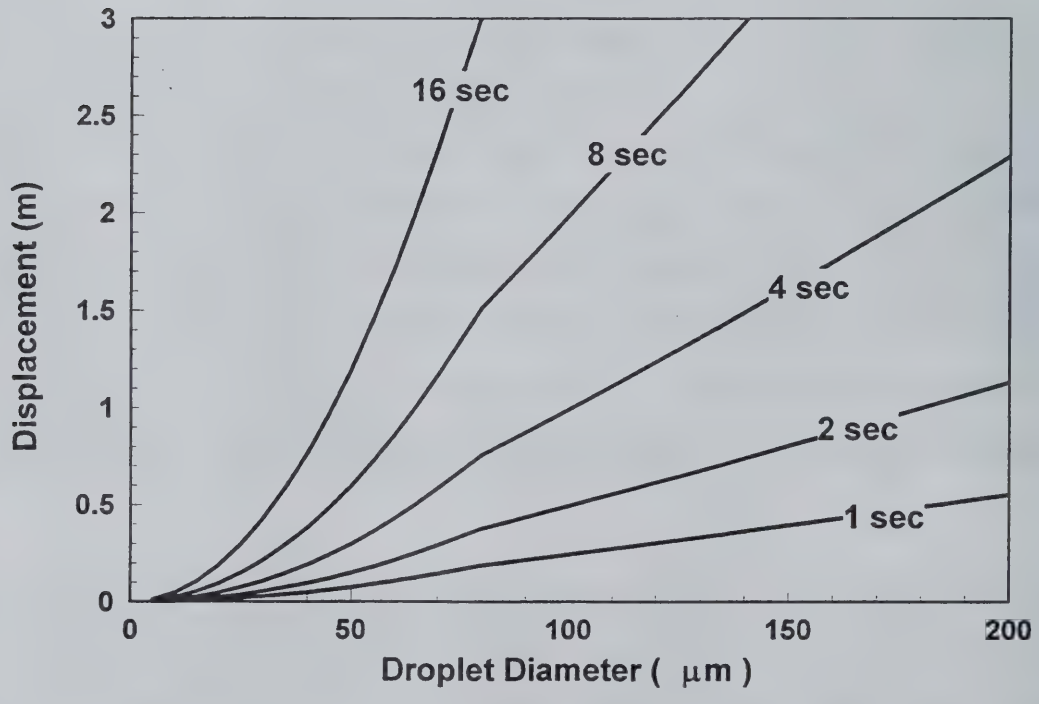

Figure 2.2 Displacement of droplets as a function of time

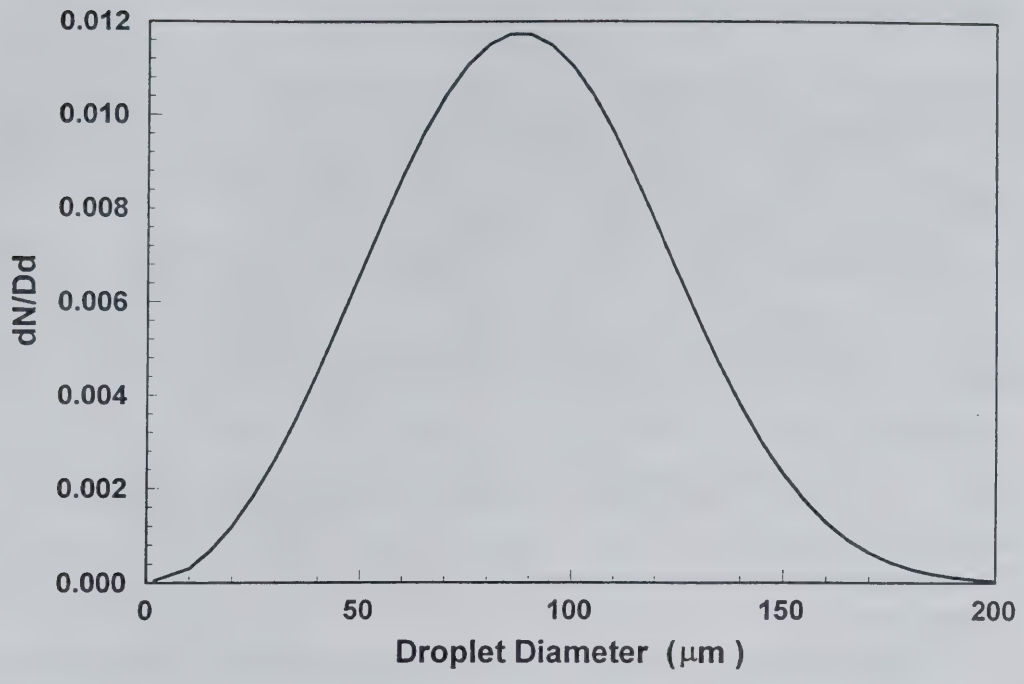

Figure 2.3 Initial droplet distribution represented by Rosin-Rammler Equation

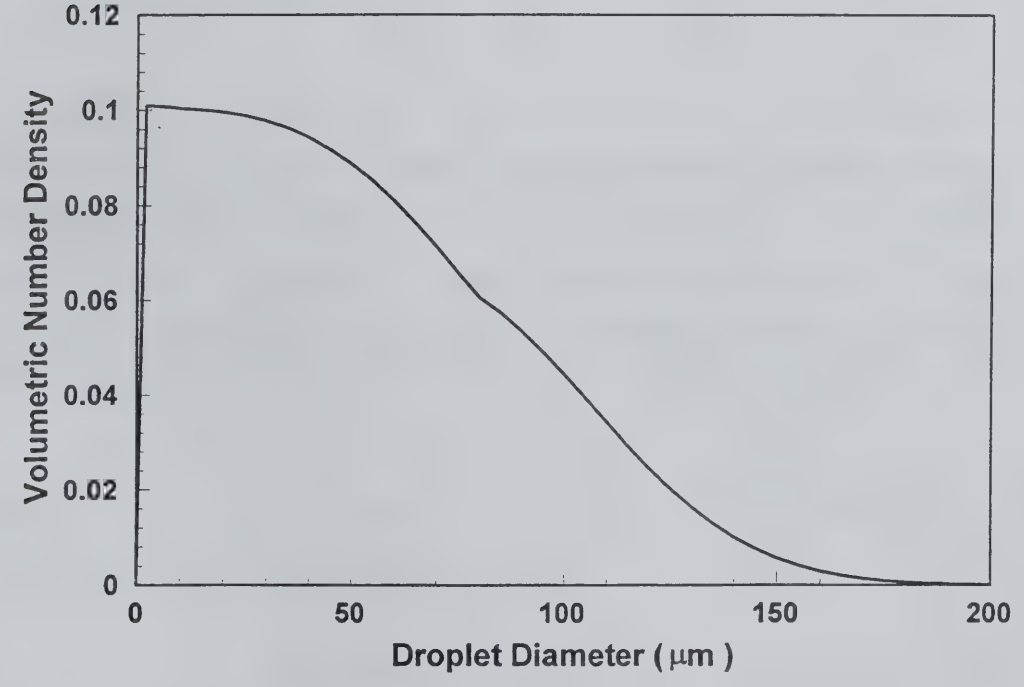

Figure 2.4 Volumetric spectrum of droplet distribution

2.1.2 Equations of the Two-Phase Transport

The transport of spray in terms of the two-phase air droplet flow is modeled numerically with a three-dimensional transient computational fluid dynamics (CFD) code. This computer code is under continued development to accommodate various spraying applications in automotive, painting, coating, and agricultural industries.

The equations for the convective transport of the gas phase are formulated by the conservation of the mass, momentum, enthalpy, turbulent kinetic energy, and energy dissipation rate of the turbulent kinetic energy for an unsteady, compressible, turbulent flow. The source terms in each of these transport equations represent the effects the droplets phase. The two phases are fully coupled through the source terms. The so-called "Eulerian-Lagrangian Scheme" is employed for the numerical modeling. The turbulent gas flow is modeled using the two-equation, k-ε method in an Eulerian coordinate; and the droplets are traced stochastically in a Lagrangian coordinate. The droplet dispersion is implemented by modeling the interaction between the gas turbulent eddies and trajectories of the droplets. The details of the formulation of the multi-phase flow can be found from Chung (1993) and Shang (1992).

The gas transport equations are solved using the transient time-averaged Navier-Stokes equations with the standard two-equation, k-ε turbulence model in an Eulerian formation. The general governing equation of the gas phase transport is given by:

$$\frac{\partial}{\partial t}(\rho\Phi) + \nabla\cdot\left(\rho\vec{U}\Phi\right) = \nabla\cdot(\Gamma\nabla\Phi) + S_{\Phi} + S_{\Phi p} \qquad (2.4)$$

The effect of the gas turbulence on the droplet transport is obtained by adding a velocity fluctuation u' to the mean gas velocity while tracing the droplets. Assuming isotropic turbulence, u' is sampled randomly from a Gaussian distribution with standard deviation of $\sqrt{2k/3}$. The k is the turbulent kinetic energy of the gas phase where the droplet is located. The droplet dispersion is implemented by modeling the interaction between the gas turbulent eddies and trajectories of the droplets in the following droplet momentum equation:

$$\frac{dv_i}{dt} = \frac{U_i + u_i' - v_i}{\tau} + \frac{F_{bi}}{m_p} \qquad (2.5)$$

where the magnitude of relaxation time, τ ,is determined by:

$$\tau^{-1} = \frac{3}{8}\frac{\rho}{r_p\rho_p}C_D\left|U_i + u_i' - v_i\right| \qquad (2.6)$$

and the C_D is the drag coefficient given by Amsden et al. (1985).

Finite difference approximations are employed to discretize the transport equations on non-staggered grid mesh systems. A third-order upwind scheme plus adaptive second-order and fourth-order dissipation terms are used to approximate the convective terms. A pressure based predictor/multi-corrector solution procedure is employed to enhance velocity-pressure coupling and mass-conserved flow field solutions at the end of every time step. A time-centered Crank-Nicholson time-marching scheme is used for the temporal discretization in the transient flow simulations.

A large number of droplet groups are traced through the flow field. Every droplet group represents a number of real droplets with the same properties and is calculated independently.

2.2 Transport of Droplets over Rectangular Strips

This section is divided into two parts in an attempt to evaluate the mist transport: First, the transport of droplets in an air flow across and in the vicinity of a single rectangular strip is investigated by using the numerical solutions of Navier-Stokes equations with droplet motions. Then, based on the flow analysis, an analytical expression is obtained to provide a quantitative understanding of the penetration of the droplets through the opening slots of an equipment compartment.

2.2.1 Computational Conditions

Numerical simulations employing the two-phase Navier-Stokes equations in a two-dimensional formulation are obtained to reveal the flow field and the droplet motions around a single rectangular strip (Fig. 2.5). This strip with a width of 0.047 m is positioned horizontally as a blocking object or an obstruction in the flow field with dimensions of a length of 0.234 m and a width of 0.563 m. Cartesian grids of 61 x 61 are used in the flow domain. The grids are non-uniformly spaced and a denser arrangement is made near the strip. The free stream velocity of the gas is 1m/s which gives the Reynolds number based on the target width ($Re_t = \rho_p D_t U/\mu$) of 3126. Droplets of uniform size distribution of 20, 50, 100, and 200 μm are uniformly injected with the gas phase across the flow field from the top of the domain. The initial injecting velocity of the droplets is the sum of the gas streams velocity and the terminal velocity corresponding to that droplet size. The relative velocity between the droplet and the gas streams is important for the effect of turbulent fluctuation. The objective is to examine the droplet trajectories above, around, and beneath the strip, and the local deposition pattern of the droplet on the strip.

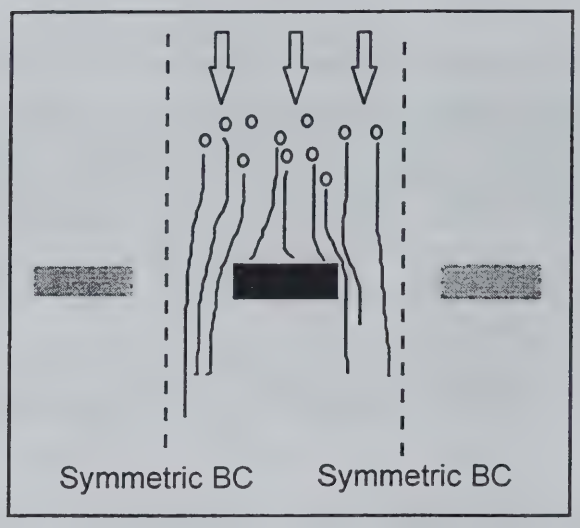

Figure 2.5 A schematic of the flow over a rectangular strip

The time step has to be reasonably small enough to capture the real trajectory of the droplets in the vicinity of the strip. If the time step is too large, the droplets tend to overshoot their trajectories. As the droplets approach the object, the larger ones may be intercepted by or impacted on the obstruction due to inertia while the smaller ones may follow the air streams closely to flow around it without impaction. However, the governing factors of this transport mechanism are the flow condition of the air streams, the properties of the droplet, and the geometry of the blocking object. In addition, it is also known that a cross flow over an object (stagnant point flow) would induce secondary flow and vortex structures downstream behind the object at a certain range of Reynolds number. Therefore, the trajectories of the droplets might be strongly influenced by the nature of wake behind the object which can usually be characterized by the alternate vortex shedding.

2.2.2 Results and Discussions

Figure 2.6 shows the typical plots of the droplet trajectories of both 50 μm and 200 μm droplets in the vicinity of a horizontal strip. Some droplets traveling from above the strip will deposit on it. In general, those droplets which deposit on the strip show different angles of impact. Smaller droplets tend to follow the air streams closely and escape from deposition; while larger droplets have more inertia and would collide with the strip more frequently. For example, when the 50 μm droplets are approaching the strip, those near the edges of the strip are driven away easily by the air streams without hitting the strip.

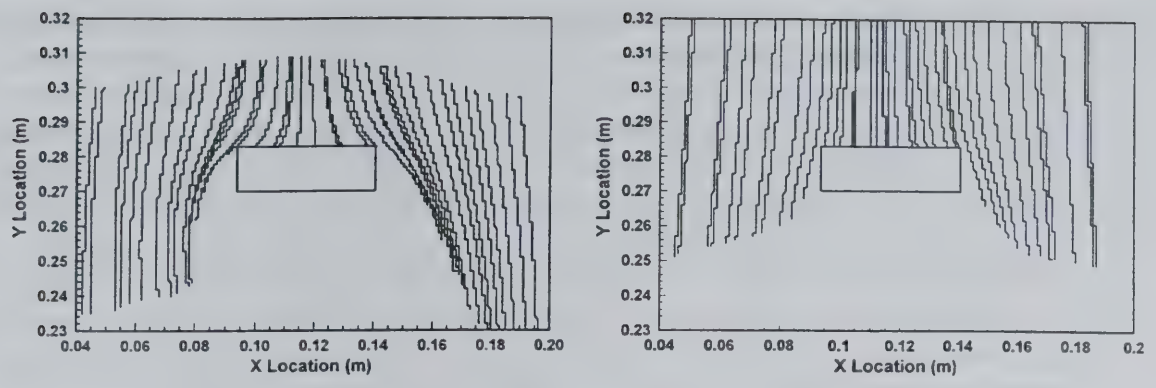

A *B*

Figure 2.6 Droplet trajectories in the vicinity of a strip (A - 50 μm; B - 200 μm)

Their local deposition patterns are found in Fig. 2.7. It shows that the 50 μm droplets exhibit more curvature of their trajectories associated with the air streams and tend to impact on the edges of the strip more often. On the other hand, the 200 μm droplets tend to move in straight lines without following the curvature of the air stream near the strip. Therefore, the overall pattern seems to be more flat for the 200 μm droplets than that of the 50 μm droplets. The deposition quantity at each location on the strip is obtained by averaging the deposition fluxes at its adjacent locations. This observation is in close agreement to those reported as the local deposition efficiency by Noll and Pilat (1970).

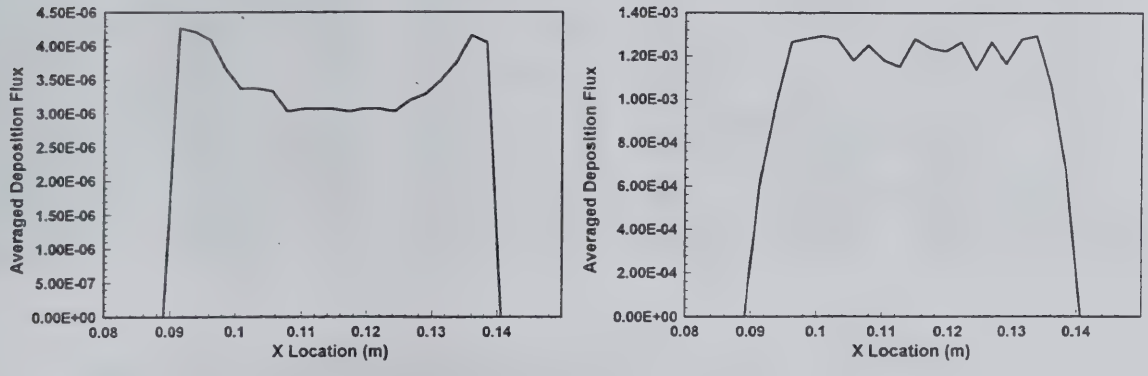

A *B*

Figure 2.7 Local deposition pattern of droplets on a strip (A - 50 μm; B - 200 μm)

The gas flow streamlines together with the instantaneous distribution of the droplets in the field are shown in Fig. 2.8 with sizes of 20 μm, 50 μm, 100 μm, and 200 μm. Entire liquid phase is present in each computation to reveal the coupling effect between the two phases. The spray is assumed to be sufficiently dilute so that the collisions between droplets can be neglected. The grids have been restructured in order to focus on revealing the flow condition beneath the strip (Fig. 2.8E).

Due to the two-way coupling between the gas and the droplet phases, the gaseous streamlines show a slight variation as the droplet size increases. Right below the strip, both the flow re-circulation zone and the vortex shedding structure appear. The re-circulation zone is of comparable size to that of the strip and very little number of droplets can be swept into the re-circulation zone due to the inertia effect. The flow wake also shows the oscillatory motion in time. Further away from beneath the strip, turbulent diffusion shall allow droplets to migrate towards the centerline and eventually may merge together to close the spray wake. However, the droplets may not follow the flow wake closely depending upon the size of the droplets and the flow condition. Small droplets of 20 μm tend to follow the gas streams closer behind the wake than the large droplets of 200 μm. The 200 μm droplets form an 'envelope' behind the strip where no droplet can be diffused in. The cases of 50 μm and 100 μm show the intermediate situations of the droplets in the wake behind the strip. When the droplet size is increased, its inertia effect becomes more important such that the droplets do not follow closely with the gas streamlines in the wake zone. Based on the above condition of Reynolds number of 3126, it can be seen that the smaller droplets have a better capability to circulate around the obstruction in order to reach the location behind it. Larger droplets have more inertia and will be less likely to reach the back side of the object.

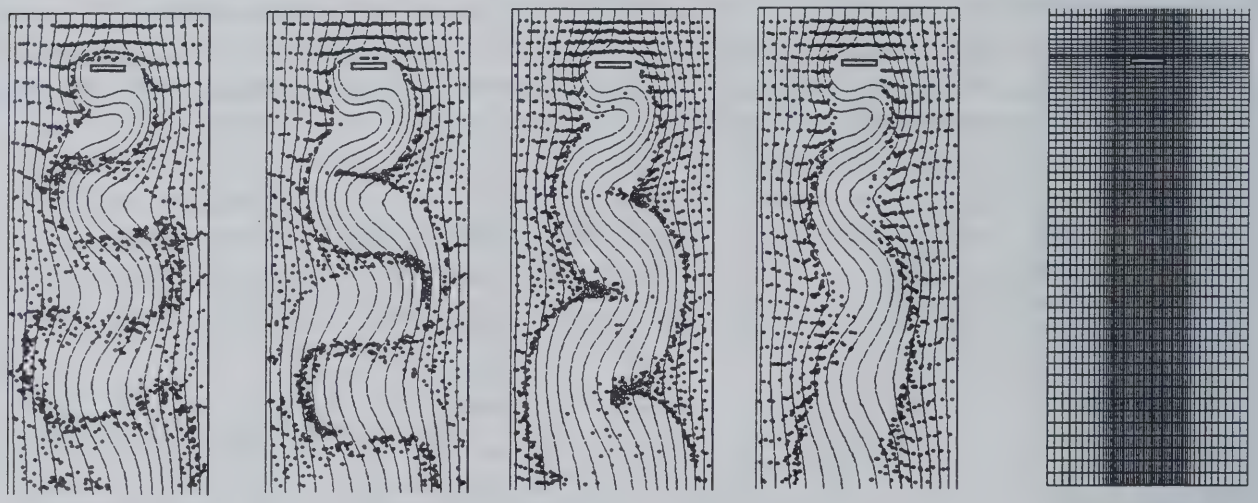

Figure 2.8 Instantaneous droplet distribution in the air streams (A - 20 μm; B - 50 μm; C - 100 μm; D- 200 μm; E - grid distribution)

2.2.3 Penetration of Droplets Through the Openings

It is of interest to determine the extent to which the droplets would be penetrating through the gaps between an array of strips. This is similar to the droplets penetration through an opening slots structure into a compartment (Hung and Yao, 1997). In theory, the mechanism of in-flight droplets penetrating through an array of openings can be closely related to the

phenomena of inertial impaction. The term 'inertial impaction' refers to the situation where droplets, due to inertia, impact directly against an object without following the curvatures of the streamline in the vicinity of the object. The inertial impaction of particles on objects such as cylinders, spheres, and rectangular strips has been examined extensively by various researchers both theoretically (Langmuir and Blodgett, 1946; Ranz and Wong, 1952; Golovin and Putman, 1962; Noll and Pilat, 1970; and Konstandopoulos et al., 1993) and experimentally (May and Clifford, 1967; Noll and Pilat, 1970; Eleftheriadis and Colbeck, 1992; and Hahner et al., 1994) for aerosol research. Among the theoretical works, the common approach to analyze the impaction characteristics and its corresponding collection efficiency on a single object was to assume a potential flow field around the object.

Little information, however, has been reported based on a computational approach to study the inertial impaction by computing the actual flow field around the objects. The most relevant and advanced work was reported by Ilias and Douglas (1989). They performed a numerical analysis of the deposition of aerosol particles on cylinder using a computational fluid dynamics framework to obtain the transient nature of the flow field around the cylinder based on full Navier-Stokes equations. Then, the motions of the droplets are numerically integrated with the flow field solutions. It was concluded in their studies that large variation of the results exists among the various approaches. In addition, the theoretical work of using potential flow to predict the flow field around the object generally over-predicts the collection efficiency while the viscous flow field grossly underestimates the results. Since the actual flow field is neither totally potential nor viscous, solving the Navier-Stokes equations together with the droplet motions will give the most realistic solutions for the actual deposition process. However, the study by Ilias and Douglas (1989) did not take into account any coupling effect from the droplet phase to the gas phase.

The present work shows several new and unique features over other related studies: First, the two-way full coupling between the gas phase and the droplet phase, i.e., the gas phase affects the droplet phase and vice versa, is implemented. In addition, the CFD framework is conducted to analyze the inertial impaction on single rectangular strip and on two adjacent strips and can also be extended to an array of strips with repeated structure.

The collection efficiency, η, on a single target can be defined as the number of droplets of a given size actually deposited onto the target to the number of droplets which would pass through the projected area of the target if the target were removed. This can be defined as follows:

$$\eta = \frac{\text{No. of droplets deposited on target}}{\text{No. of incoming droplets over target}} \qquad (2.7)$$

Conventionally, the collection efficiency is a function of a non-dimensional number named the inertial impaction parameter, K. Based on Stokes law (May and Clifford, 1967), the stopping distance, i.e., the distance that the droplet would penetrate through a stagnant fluid when given an initial velocity, U, is given by:

$$\lambda = \frac{\rho_p D_p^2 U}{18\mu} \tag{2.8}$$

Then, the impaction parameter can be defined as the ratio of the stopping distance to the width of the target:

$$K = \frac{\lambda}{D_t} = \frac{\rho_p D_p^2 U}{18\mu D_t} = \frac{1}{18}\left(\frac{\rho_a D_t U}{\mu}\right)\left(\frac{\rho_p}{\rho_a}\right)\left(\frac{D_p}{D_t}\right)^2 \tag{2.9}$$

This dimensionless impaction parameter K can also be interpreted as a product of the target Reynolds number ($\rho_a D_t U/\mu$), the density ratio of the droplet to the surrounding air, and the squared ratio of the droplet size to the target size.

Figure 2.5 shows the schematic of the flow configuration of a compartment opening. The computation is made in a 2-D flow domain. Both sides of the domain are set to be the symmetric boundaries. This would allow the flow over an array of strips to be reduced to an isolated strip. However, an immediate concern arises to examine the effect of the width of the strip relative to the width of the flow domain (i.e., the spacing between the array). Therefore, a blockage fraction (B) is defined as below:

$$B = \frac{\text{Width of blockage}}{\text{Width of flow domain}} \tag{2.10}$$

Equation (2.10) gives a geometric measure of the width ratio of the blockage relative to the flow domain. For example, if an array of 3 strips, each has a width of 5 mm at a distance of 10 mm apart, is placed in a 45 mm wide of flow domain, then the blockage fraction will be 0.33.

Due to the repetition of the array structure, in this study, a single rectangular strip of 5 mm width is located in the center of the flow domain. Five widths of flow domain namely, 7.5 mm, 10 mm, 15 mm, 25 mm, and 35 mm, are examined for the same strip to study the effect of array spacing. The total length of the domain is kept constant at 50 mm. Three velocities of the incoming air stream are selected: 0.5 m/s, 1 m/s, and 2 m/s, and the corresponding target Reynolds numbers are 167, 334, and 667, respectively. Droplets of a given size are injected uniformly across the flow field during each simulation. The sizes of the droplets considered are 10 μm, 20 μm, 50 μm, and 100 μm.

The trajectories of the droplets are monitored. Once the droplets are on the strip, they are deposited and are then taken out from the computation domain. The total number of droplets injected directly from above the strip and the number of those droplets deposited onto the strip are both recorded. For consistent results, the simulation of each case is repeated for 3 times. Therefore, the average collection efficiency based on the 3 trials for each K value is obtained using equation (2.7).

Since a typical compartment opening would consist of an array of repeated slots, there is a need to validate the use of a single object to represent multiple slots. Therefore, another case of flow over two strips in a 30 mm flow domain is also investigated, with each strip having the same width of 5 mm at a distance of 10 mm apart. The results from this case are compared with the case of the single strip in a 15 mm flow domain. Both cases have the same blockage fraction of 0.33. From Fig. 2.9, the collection efficiencies of both situations are almost identical, indicating that the collection efficiency of double strips can be reasonably approximated by that of a single strip. Plotting the collection efficiency (η) against the impaction parameter (K) on a semi-log scale would give a typical deposition "S" shape curve. The higher the K values, the higher the collection efficiency would be. To analyze the effect of blockage fraction on the collection efficiency, five different values of B, namely, 0.14, 0.2, 0.33, 0.5, and 0.67, are examined. The comparisons are shown in Fig. 2.10. When blockage fraction is less than 0.33, the curves are very close to each other.

The case with B equals 0.33 is compared to other published works by various researchers and is shown in Fig. 2.11. The current results compare well with the theoretical results obtained by Langmuir and Blodgett (1949) and by Ranz and Wong (1952), both based on the potential flow solutions. Therefore, it can be concluded that if the width of the strip is less than about 33% of the width of the flow domain, the collection efficiency would not be affected significantly by the spacing between an array of strips.

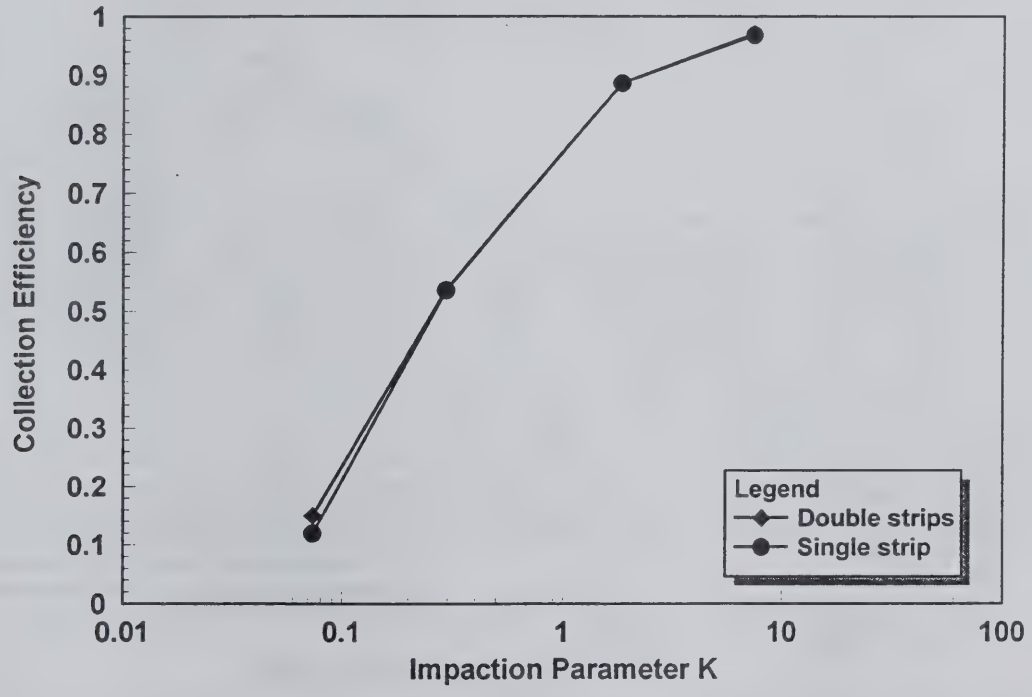

Figure 2.9 Comparison of collection efficiency of single strip verses double strips (B = 0.33)

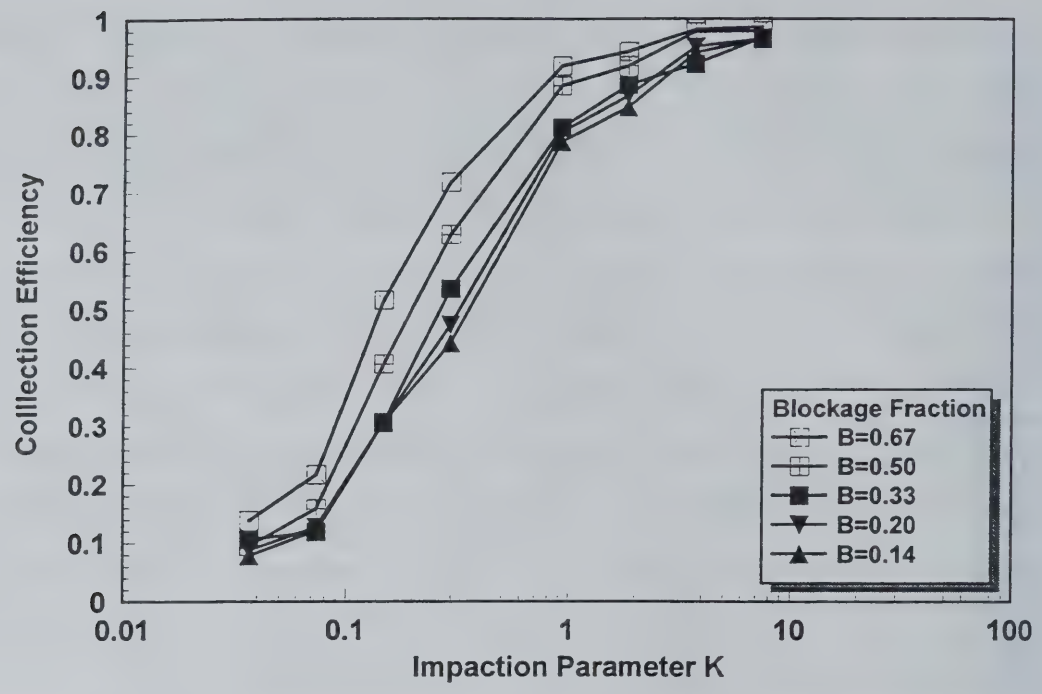

Figure 2.10 Effect of blockage fraction on the collection efficiency on rectangular strip

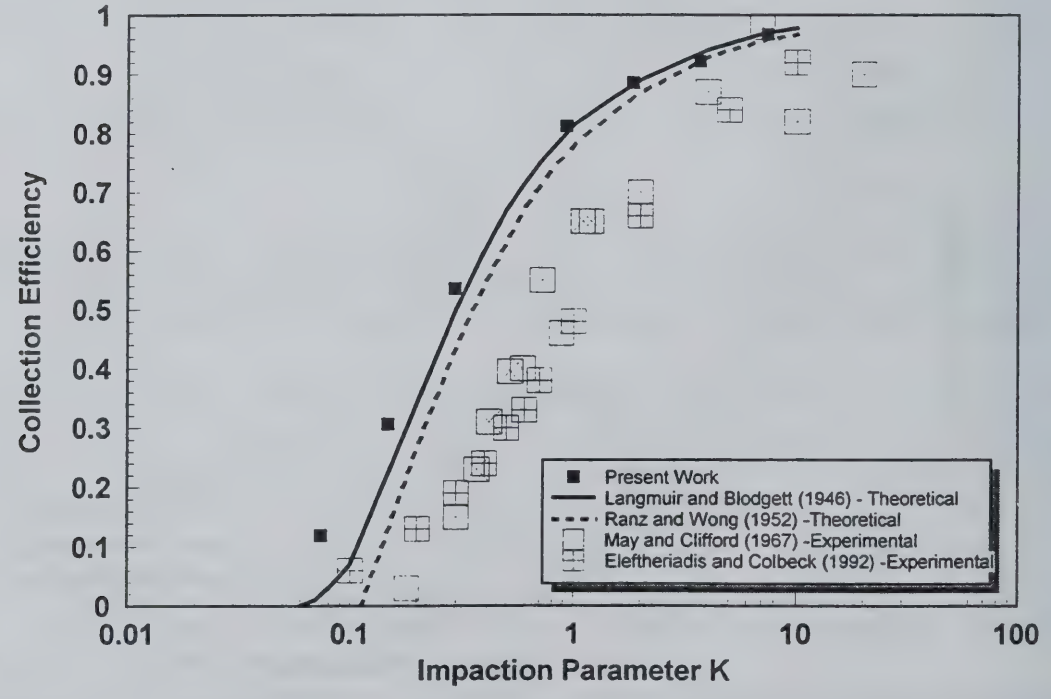

Figure 2.11 Collection efficiency of a rectangular strip due to inertial impaction

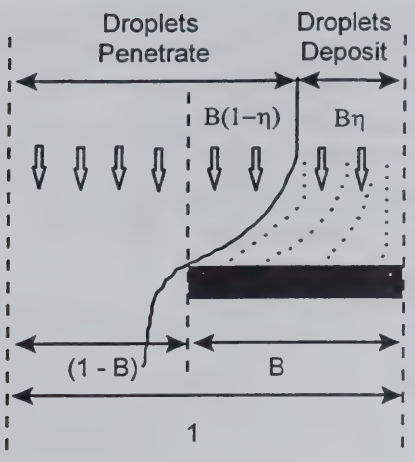

Figure 2.12 Illustration of droplets penetrating through the opening slot adjacent to the blockage

To make use of the results of the present analysis for the prediction of mist penetrating through openings, geometric consideration should be made. As shown in Fig. 2.12, for those droplets do not deposit on the target, they will follow the air stream and penetrate through the openings. The penetration efficiency can be developed to measure the amount of by-passing droplets. Assuming that the droplets are at a given size and of uniform distribution across the flow domain initially, the penetration efficiency (α) can be formulated as follows:

$$\alpha = (1 - B) + B(1 - \eta) \tag{2.11}$$

where the η is the collection efficiency and the B is the blockage fraction. The first term of the right hand side, 1-B, is the measure of droplet penetration due to the geometry effect of the opening. It is essentially the opening fraction of a given geometric condition. The second term is the additional droplet penetration induced by the flow going around the strip.

The strip covers a fraction B of the flow domain. The term 1- η is the fraction of drops which does not deposit on the strip in this region. When η tends to zero, no droplet will deposit on the block and then α will become unity. On the other extreme, when η is very close to unity, the second term vanishes and α will become 1-B. Therefore, the theoretical limiting bounds of the penetration efficiency can be found in the following relationship:

$$(1 - B) \leq \alpha \leq 1 \tag{2.12}$$

Using the collection efficiency curve of B equals 0.33 (from Fig. 2.10), the curve of the penetration efficiency verses K is calculated using equation (2.11), and is shown in Fig. 2.13. It can be seen that the collection efficiency decreases as the penetration efficiency increases. The prediction based on equation (2.11) is in close agreement with the actual numerical

simulation, as shown in Fig. 2.13 as the data points. A maximum difference of about 5% between the prediction and the actual computation is observed at high K values. As illustrated in Fig. 2.13, for large drops or at high velocity, the K value is high and the collection efficiency is very close to unity. In this situation, the droplets have higher momentum and inertia and they tend to move in straight lines. The droplets going in the straight lines would eventually either impact the strip or escape due to the geometric fraction of the blockage. Therefore, the minimum value of the penetration efficiency will be simply equal to 1-B.

On the other hand, for small drops or at a low velocity, the K value is low. The droplets possess very little inertia, the collection efficiency is close to zero. The air streams in the vicinity of the strip tend to drive the droplets away from the strip, and almost all of the droplets will not deposit on the strip and eventually penetrate through the slot. This gives a high low value of η but high α. Therefore, the maximum penetration efficiency will be very close to unity.

At other blockage fractions, a series of curves of the penetration efficiency verses the impaction parameter can be developed as shown in Fig. 2.14. The curves for B equals 0.67 and 0.5 are based on their own collection efficiencies shown in dotted line, while the remaining cases are based on the collection efficiency of B equals 0.33 as indicated by the solid line. Each of the predicted curves is also bounded by its corresponding minimum penetration efficiency of 1-B and the maximum value of unity.

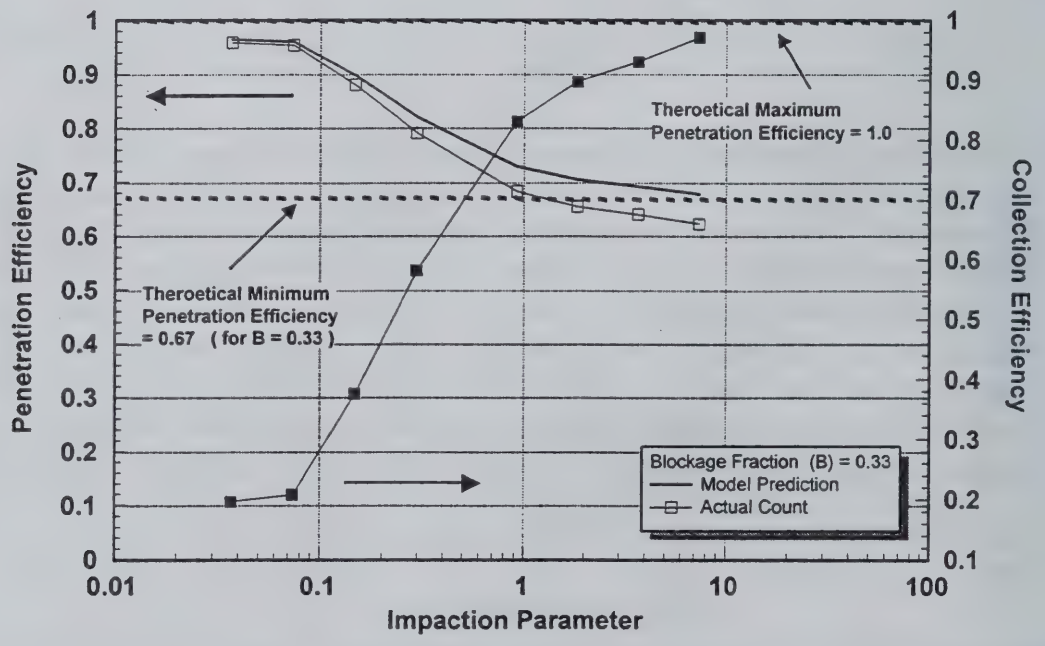

Figure 2.13 ***Penetration efficiency of droplets with blockage fraction of 0.33***

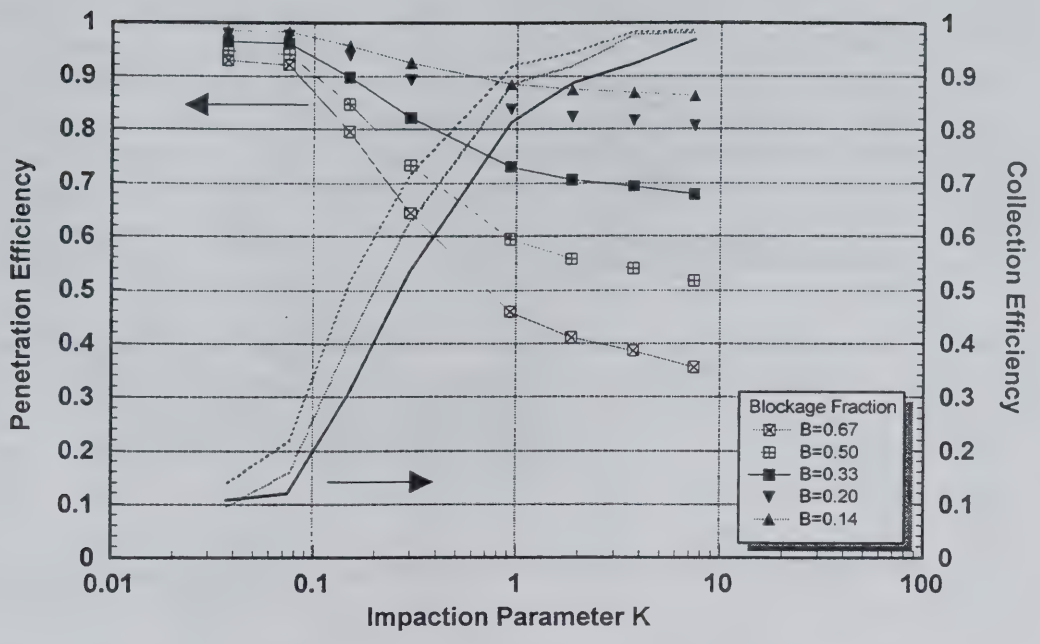

Figure 2.14 Penetration efficiency for various values of blockage fraction

2.3 Transport of Droplets over a Screen Object

The transport of droplets through a screen object is commonly encountered in many distillation processes. As expected, some droplets may pass through the mesh openings of the screen directly while others may be intercepted by the screen. The penetration and deposition of the droplet phase are strongly influenced by the motions of the droplets, coupled with the gas streams, in the vicinity of components of the screen. Since a screen structure has a rather complicated configuration and many small length dimensions, it is extremely difficult to simulate the flow to the entire screen structure without sacrificing the details of the local interactions. Therefore, for an efficient computational approach, the current investigation focuses on the droplet transport over a local portion of a screen structure, as demonstrated in Fig. 2.15 for the flow analysis. It is believed that the analysis here can also be applied to a more global screen structure in a reasonable manner. The actual droplet impaction experiments are presented in Chapter 5.

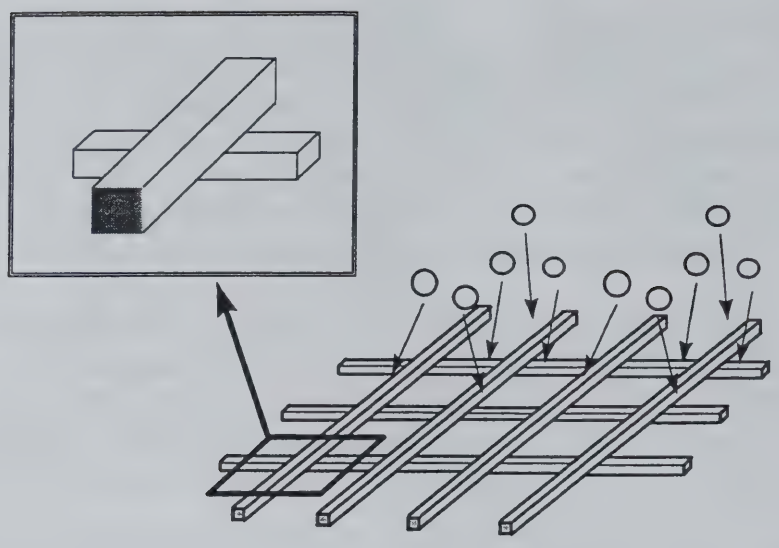

Figure 2.15 A schematic of droplet flow over a typical screen structure

2.3.1 Computational Conditions

Numerical simulations of droplet transport in a 3-dimensional configuration are presented for a situation of a screen object. Figure 2.16 displays the 3-D view of the top portion of the overall computational domain. Two rectangular blocks, each with a square cross-section, are positioned in a perpendicular orientation. These blocks represent a local region of a screen structure. Even though a screen object is typically made up of cylindrical wires, it is believed that the flow over the square blocks would reveal a basic understanding for the flow over the wires at similar conditions. In fact, similar phenomena and efficiency of the inertial impaction were reported for both the square block and the cylindrical surface (Golovin and Putnam, 1962). The deposition pattern on a wire, in general, might be slightly different than that on a flat block surface due to the difference in the geometry. The experimental aspect of the impaction of droplets on screen objects is presented in Chapter 5.

The dimensions of each block are 0.005 m x 0.005 m x 0.025 m. The overall flow domain contains a rectangular space with dimensions of 0.025m x 0.075m x 0.025m (length by height by width). Cartesian grids of 40 x 68 x 40 are used for the flow field analysis. As in the previous case, the grid distributions are non-uniformly spaced such that finer mesh arrangements are made near the blocks. The incoming gas flow velocity is selected to be at 1 m/s downward. The droplets are injected from above uniformly with a uniform size distribution with 10 μm in diameter.

2.3.2 Results and Discussions

Figure 2.17 displays the instantaneous droplet distribution in the middle plane which cuts through the middle block parallel to the flow domain. For the droplets injected directly from above the block, they all deposit onto the top surface. At the downstream locations of the

blocks, there are some droplets migrated into this middle plane due to the wake effect and the turbulent diffusion. Note that right below the lower block, there are some droplets being merged into the wake zone below, possibly due to the existing flow re-circulation zones.

The trajectories of the droplets passing over the blocks are displayed in Fig. 2.18. This figure shows that there are some droplets that are deflected away from depositing onto the block due to the inertial impaction effect described in earlier section. In general, those droplets deposited on the surface show different angles of impaction, indicating that the local deposition pattern may be a non-uniform profile, in accordance with the results shown in Fig. 2.19.

The penetration efficiency, α, of this 3-D double block configuration can be determined by directly counting the number of droplets deposited on to the blocks, using equation (2.7), through the 3-D simulation. However, in many other situations, it may not be easy to carry out the actual 3-D computations to obtain this information, due to the limitation in computing power. On the other hand, it has been shown before from equation (2.11) that the penetration efficiency is simply a function of the collection efficiency, α, and the blockage fraction, B. Therefore, equation (2.11) may actually be used to predict the 3-D penetration efficiency based on a configuration of a 2-D rectangular strip with a comparable characteristic width. The purpose of this demonstration is to examine the applicability of this equation in predicting the 3-D situations.

For the 10 μm droplets moving with the gas streams downwards at 1 m/s, the actual 3-D penetrating efficiency (α) was computed to be 0.948. The blockage fraction, B, for this 3-D configuration is found to be 0.36. The collection efficiency (η), based on the strip which has the same width as that for the block, is 0.18 from the 2-D simulation. Therefore, using equation (2.11), the corresponding 3-D penetration efficiency is found to be 0.935. These two values seem to be within reasonable comparison with a difference of 1.4%. Therefore, this illustration has demonstrated that the use of the formulation, equation (2.11) based on the 2-D collection efficiency and 3-D geometry consideration, to predict the 3-D penetration efficiency may seem to be a justified approach.

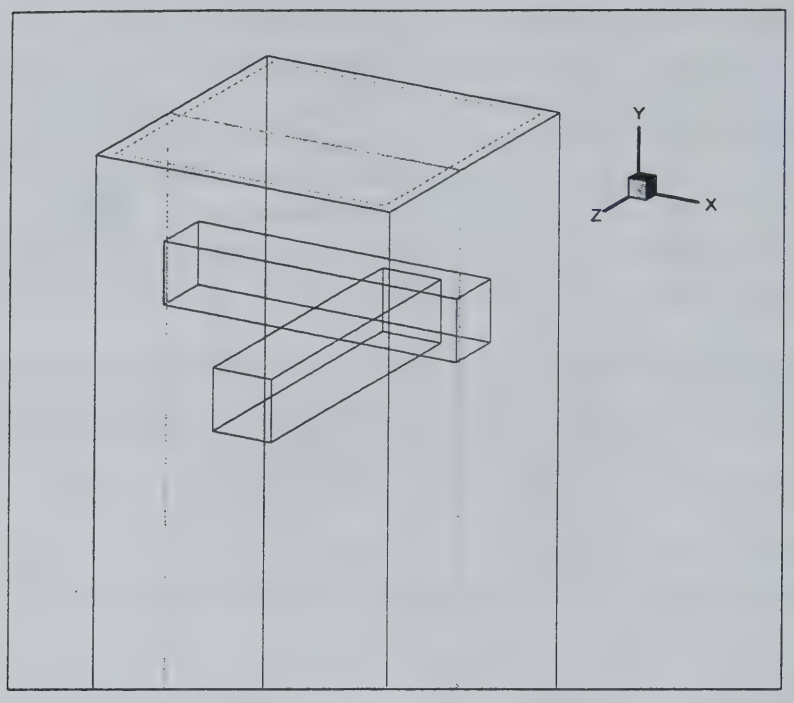

Figure 2.16 A schematic of the computational domain for the cross-block structure

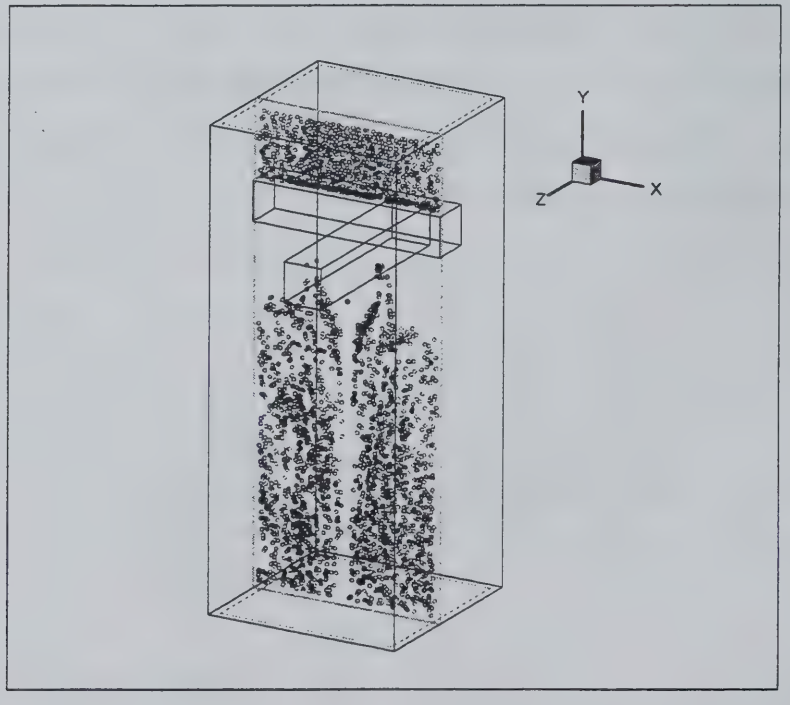

Figure 2.17 Instantaneous droplet distribution in the middle flow field

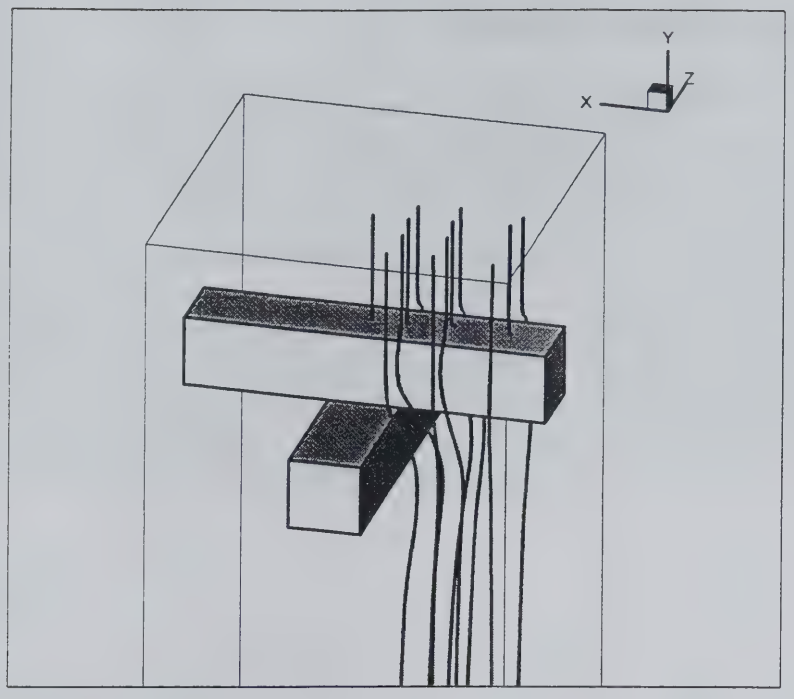

Figure 2.18 Trajectories of droplets passing over the rectangular blocks

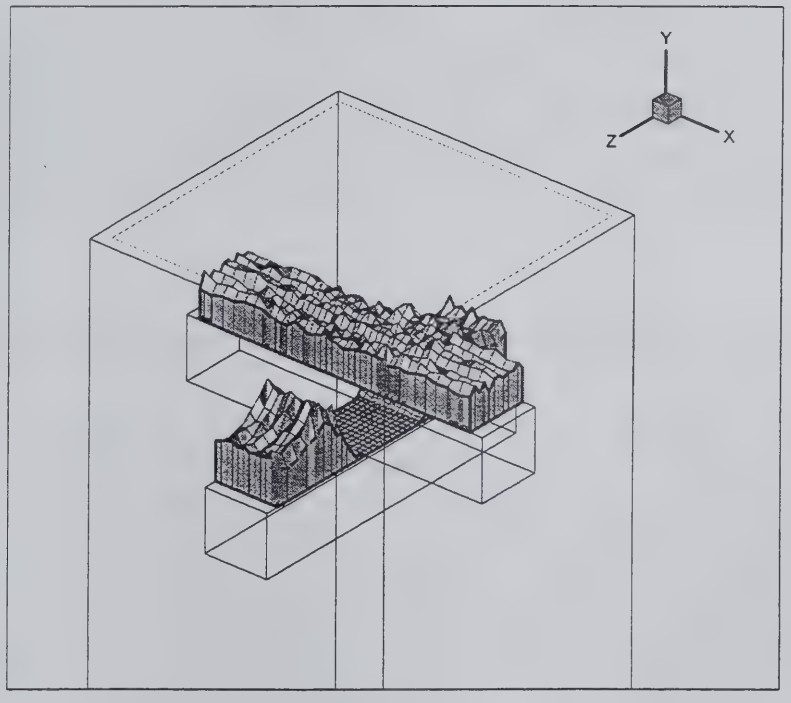

Figure 2.19 A deposition pattern of droplets on the blocks

2.4 Concluding Remarks

The use of numerical modeling to investigate the transport of droplets with the gaseous streams around the objects with complex geometry in an isothermal condition was demonstrated. It was successful to provide the visualization of the droplet distribution in the flow domain and their deposition patterns on the surfaces of the objects.

The non-dimensional impaction parameter was a good way to determine the deposition characteristic on the object. The penetration efficiency of droplets through an array of objects could be formulated using the collection efficiency (η) and geometry consideration (B). It had been demonstrated, by the screen situation, that the penetration efficiency of a 3-D complex screen object could be approximated by using the collection efficiency of the 2-D rectangular strip with similar characteristic dimension through equation (2.11). The prediction was found to be of reasonable agreement.

Chapter Three

Experimental Setup And Procedure

Summary

This chapter presents the details of the overall experimentation for the droplet impaction studies. First, the principle of producing mono-size droplets is reviewed in order to explore the design criteria for generating the droplets of desired conditions. Then, two mono-size droplet generators are designed and implemented. The overall setup for the experiments as well as the experimental conditions are also discussed.

3.1 Background

Fine droplets are traditionally generated by forcing liquid through a nozzle under pressure or through the air-assisted atomization in twin-fluid atomizers. In either case, the sprays are usually formed in a polydisperse drop size distribution, which may not be desired in some spray applications. For example, in order to maintain the quality of ink-jet printing precisely, there is an absolute need to generate droplets on a well controlled basis, preferably in a very narrow droplet spectrum or even mono-disperse drop size distribution. Therefore, it is important to identify the optimal and limiting conditions for mono-size droplet generation based on a well documented theory. This chapter is devoted to the principle for the production of mono-size droplets and the overall experimental setup and conditions for the impaction study. The results for the impaction experiments are presented in the next 2 chapters.

3.2 Principle of the Production of Mono-size Droplets

The break-up of liquid jet into uniform droplets was first investigated by Savart experimentally in 1833. He observed that a liquid jet in cylindrical form becomes unstable if its length is larger than its circumference. This is because a laminar liquid jet exiting from a nozzle is subjected to some natural frequencies associated with the jet. This disturbance will lead to a natural breakup of the liquid jet. Later, the theoretical work of disintegrating a liquid jet into droplets was examined by Lord Rayleigh in 1879. He showed that a cylindrical liquid jet will become dynamically unstable under the action of surface tension. He then derived the optimal wavelength disturbance (λ_m) which leads to the most rapid disintegration of the cylindrical jet into uniform-sized droplets:

$$\lambda_m = 4.508 D_j \qquad (3.1)$$

where D_j is the diameter of the liquid jet.

Schneider and Hedricks (1964) experimentally determined the range of λ that could generate uniform droplets:

$$3.5D_j < \lambda < 7.0D_j \tag{3.2}$$

It is a practical interest to find out the relationship between the size of the orifice and the diameter of the uniform droplets. This relationship can be determined first by considering the experimental work of Linblad and Schneider (1965). They showed that the relationship between the liquid jet diameter and the inside diameter of the capillary tube (orifice) was approximately:

$$D_j = 0.8D_o \tag{3.3}$$

where D_o is the diameter of the orifice.

To control the break up process, artificial disturbance can be applied to the jet with amplitude larger than the natural disturbance. The mechanical disturbance can be transmitted to the liquid jet by the means of some vibrating devices, such as a piezoelectric transducer. The frequency of the pulse to be applied to the transducer can be found from the wave equation:

$$f = \frac{V_j}{\lambda} \tag{3.4}$$

where V_j is the velocity of the jet. The minimum velocity needed to form a jet from a capillary tube was derived by Linblad and Schneider based on the conservation of energy approach as:

$$V_j = \left(\frac{8\sigma}{\rho_l D_j}\right)^{1/2} \tag{3.5}$$

Schneider (1964) showed that when the jet is disturbed, the mass of each droplet with diameter d is equal to each undulation with a wavelength of λ, that is,

$$M = \frac{\pi D_j^{\,2}}{4}\rho_l\lambda = \frac{1}{6}\rho_l\pi d^3 \tag{3.6}$$

Equating the above expression will give the diameter of each droplet to be:

$$d = (1.5 D_j^2 \lambda)^{1/3} \tag{3.7}$$

Substituting the optimal wavelength $\lambda = \lambda_m = 4.508 D_j$ for the most rapid instability, the drop diameter and the jet diameter can be related as:

$$d = 1.89 D_j \tag{3.8}$$

Finally, the droplet diameter at a given size of orifice under the above condition is found to be:

$$d = 1.512 D_o \tag{3.9}$$

Equation (3.9) gives the relationship of the size of the droplet for a given orifice operating at the optimal condition. Meanwhile, the range of operating condition for droplet generation can also be deduced from the above equations.

3.3 Design of the Mono-size Droplet Generator

Mono-size droplets can be generated using a variety of mechanisms. This section presents the two devices which generate mono-size droplets through the piezoelectric vibration.

3.3.1 Mono-size Droplet Stream Generator

The mono-size droplet stream generator was designed based on the Impulsed Liquid Spray Generator developed by Ashgrizzadeh and Yao (1983). The operation of this generator is based on the theory of the Rayleigh-type breakup of liquid jets which has been described in details in the previous section.

Figure 3.1 displays the details of this droplet generator used for the experiments. It consists of a fluid chamber, a piezoelectric crystal (Model 104-95NS, Piezo-electric Product Inc.) glued on a thin brass plate mounted on top, and an orifice plate mounted on the bottom. In some situations, this bottom orifice plate is replaced by another plate with a glass nozzle attached. Distilled water from the reservoir is pumped into the droplet generator. As the fluid chamber inside the droplet generator is pressurized, a liquid jet is formed through the orifice. Electric pulse signal, monitored by an oscilloscope (Tektronix, 2211), from the pulse generator (Tektronix, CFG250) are then applied to the piezoelectric plate. When the piezoelectric plate is charged with pulses, it vibrates rapidly. The rapid vibration creates disturbance which is imposed on the liquid jet. Therefore, the liquid jet then disintegrates into fine water droplets with uniform size, spacing, and velocity.

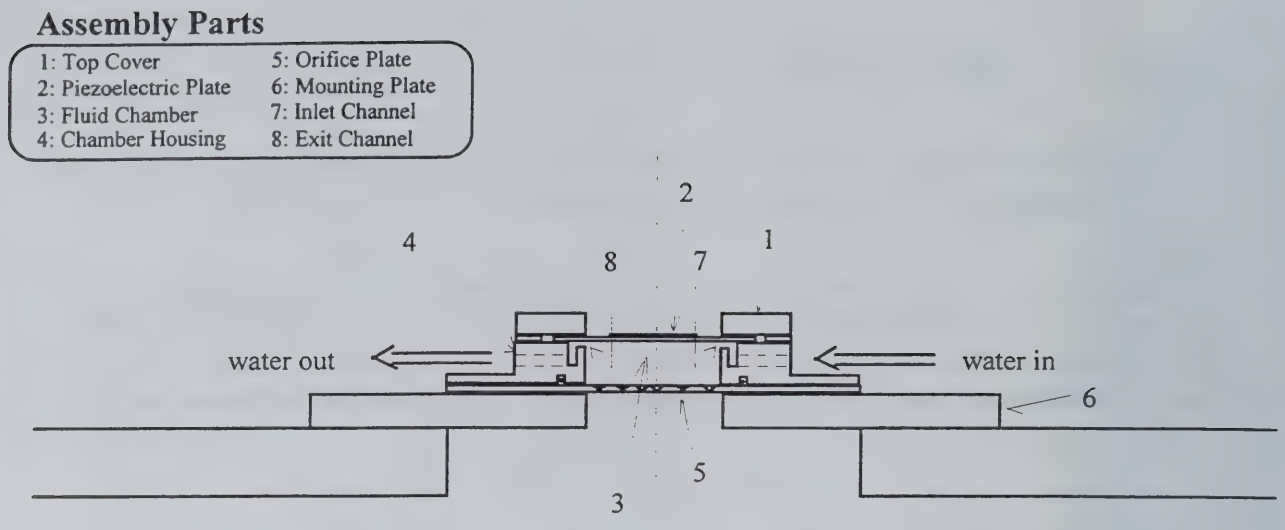

Figure 3.1. Schematic of the mono-size droplet stream generator

There are some design considerations for the mono-size droplets to be generated successfully. First, the interior of the fluid chamber has to be machined smoothly because any sharp corners or edges in the fluid chamber may create small cavities during pulsation and then reduce the magnitude of the pressure pulse generated by the piezoelectric vibration. In addition, the exits of the orifice or glass nozzle have to be smooth and round enough because any burrs or rupture around the edges will destroy the formation of the droplet stream. Finally, any residual air bubbles trapped into the chamber would also diminish the effect of pressure pulses by the piezo-electric vibration. Therefore, special inlet and exit channels of water flow are implemented in the fluid chamber for the bubbles to be swept away naturally.

Figure 3.2 displays the behavior of the droplet stream subjected to piezoelectric vibration. Both close-up and far-view pictures are included. In Fig. 3.2A, when there is no artificial disturbance applied to the jet (i.e., when the piezoelectric vibration is turned off), the liquid jet clearly breaks up into droplets with random sizes and spacing. However, as shown in Fig. 3.2B, when the piezoelectric vibrations are applied to the jet, the jet disintegrates into uniform droplets with equal spacing. The stream shown here has a droplet diameter of about 680 μm moving at about 2 m/s. The corresponding piezoelectric vibration frequency is about 1000 Hz.

A. Without piezoelectric vibrations

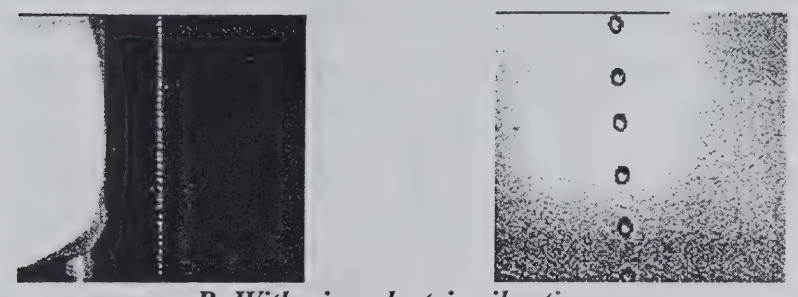

B. With piezoelectric vibrations

Figure 3.2 Operation of the mono-size droplet stream generator

3.3.2 Mono-size Drop-on-Demand Droplet Generator

Another mono-size droplet generator has also been designed to accommodate the need of generating droplets on an individual basis. Therefore, a drop-on-demand (dod) droplet generator has been implemented (Yang, 1996). Its components are almost identical to the droplet stream generator described in previous section. The unique feature of this drop-on-demand generator is its superb control of droplet injecting frequency. When an electric pulse is applied to the piezoelectric crystal, it vibrates once, giving a repulsive force at the nozzle exit through the fluid chamber to form a single droplet. This droplet generator is capable of producing droplets up to 10 Hz. The size of the droplet is generally very close to that of the nozzle diameter which, at the present experiment, is between 100 μm to 300 μm.

Unlike the previous stream generator, this drop-on-demand generator requires an extremely careful control over the pressure balance between the reservoir and the nozzle exit. In addition, the voltage supplied for the pulses is usually very high, typically ranging from 50V to 80V peak-to-peak.

3.4 Experimental Setup and Conditions

The schematic diagram of the overall experimental setup is displayed in Fig. 3.3. During the experiment, distilled water from the liquid reservoir was pumped into the droplet generator. A rotameter with a control valve was used to regulate the volumetric flow rate. The main

components are the mono-size droplet generator, the distilled water loop, and the image recording unit for data analysis.

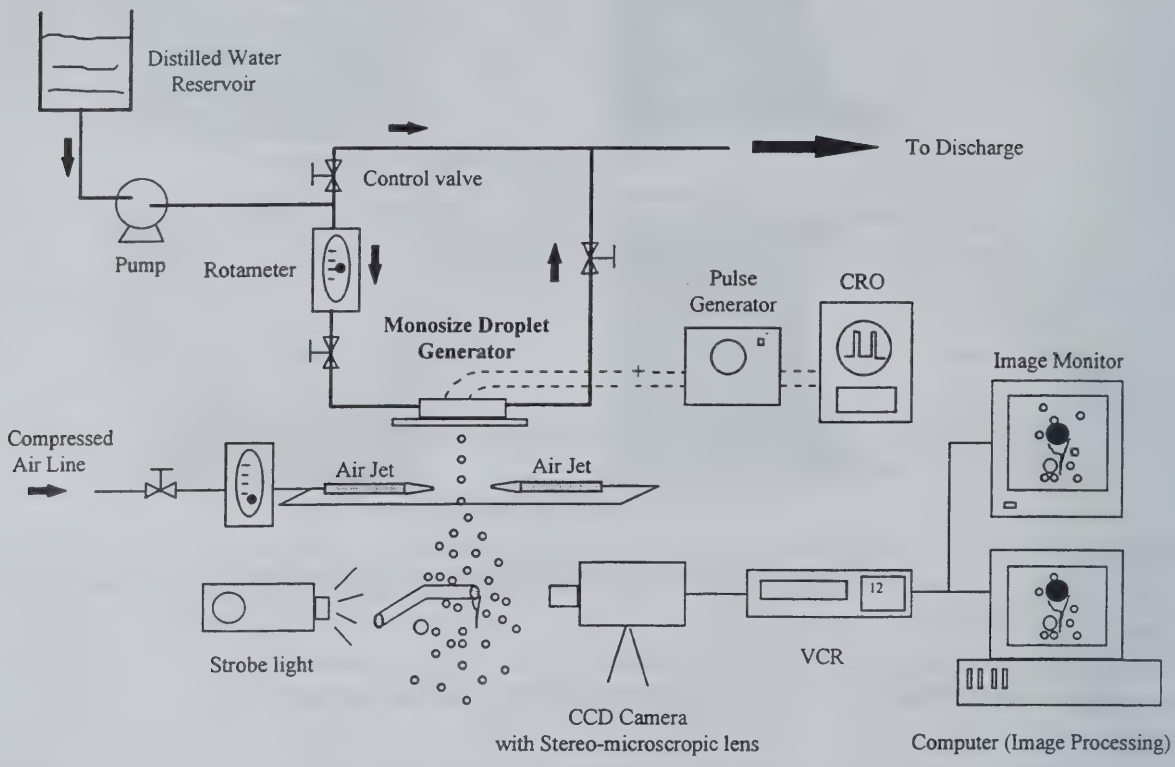

Figure 3.3 The overall experimental setup

The velocity of the droplet is determined by measuring the jet diameter and the volume flux. In addition, Beckwith and Marangoni (1990) provided an alternative method which can be used to determine the real frequency of the droplet stream as follows: Adjust the flashing frequency of the strobe light to 'freeze' the images of droplet stream in space. Then, the first frequency f_1 and the next lower frequency f_2 can be used to deduce the real frequency of the droplet stream, f_t,:

$$f_t = \frac{f_1 \times f_2}{(f_1 - f_2)} \tag{3.10}$$

Once the spacing between the centers of two droplets, l_d, is evaluated from the image, the velocity of the droplet is the product of this spacing and the real frequency of the droplet stream:

$$V_o = l_d \times f_t \tag{3.11}$$

The droplet velocity is also determined by this method to confirm with that from the first one. Both results are in good agreement.

In order to randomize the droplet stream, two small opposing air jets are used to perturb the droplet stream at about 5 cm below the nozzle exit. The droplets become more randomly spread when they approach the object. The droplets impact on to the object which is located about 10 cm below the orifice. The images of the impacting phenomena are displayed on a high resolution image monitor (Sony, PVM-1271Q) using a CCD camera (Javelin, Newvichip) equipped with a high magnification stereo-microscopic lens (Nikon, SMZ-10) and are recorded simultaneously on a video tape by a VCR. The illumination is provided by a background strobe light (Strobotac, 1531-A) of 10 ms pulse duration. The selected images from the video tape are captured into a Pentium Pro 200 MHz computer using a frame grabber. These images are then analyzed frame by frame through digital image processing software (Bioscan Optimas).

The digital images are also used for the size measurements of the droplets hanging or dripping from the objects. Once a known length has been used for calibration, this calibrated scale can then used to measure the drop size. At least 5 pictures of each condition are used for obtaining a representative averaged data measurement.

In the first experiment, a droplet stream of 680 μm in diameter was generated to impact on wires at regular offset distances. The incoming velocity of the droplet stream was measured to be about 2.0 m/s. This stream of droplets was made to impact on wires at various regular offset distances.

In the second experiment, a stream of mono-size water droplets with smaller diameter of 350 μm was also generated using the same droplet generator. This stream was perturbed by two small opposing air jets to randomize the spread of the droplets when they approached the wires. This impaction experiment was for random offset distance. The velocity of the droplet was determined by measuring the jet diameter and the volume flux which gave the incoming four velocities ranging between 2.8 m/s and 7.0 m/s. The values of the droplet Weber number corresponding to the velocities were 40 and 230, respectively. Under these conditions, the piezoelectric plate was vibrating at a frequency between 3700 and 9000 Hz, respectively, with a constant amplitude of 20 Volt PP. The volumetric flux was determined by directly collecting the local flux at the location where the screen was positioned. It was measured to be about 17.6 $cc/min/cm^2$. This volumetric flux was selected for experimental convenience under the current conditions.

In the third experiment, a second droplet generator was also designed to operate at a drop-on-demand condition. In this case, single droplets of about 110 μm in diameter were generated with droplet velocity of about 1 m/s at a rate up to 10 drops per second. The single droplets were made to impact on wires at a well controlled droplet frequency and offset distance.

The target objects for the impaction experiments were the stainless steel wires and wire screens. Seven wires with diameters ranging from 113 μm to 1588 μm were used for the wire experiments. For the screen experiments, twenty plain woven wire screens with different wire diameter and mesh opening were chosen, ranging from a coarse screen of 2 meshes per inch length with diameter of 1.6 mm to a fine screen of 100 meshes per inch length with wire diameter of 0.14 mm. The experimental results are presented systematically in Chapters Four and Five.

Chapter Four

The Impaction of Droplets on Horizontal Wires

Summary

This chapter presents an experimental investigation of the water droplets impacting on cylindrical wires at isothermal condition. Mono-size droplets of 110, 350, and 680 μm in diameter were generated using piezoelectric droplet generators. The droplets were made to impact on wires with diameters from 113 μm to 1588 μm either at a regular offset distance or at random offset. Generally, the droplet impacting phenomena include disintegration and dripping. If the incoming droplets are larger than the wire, finer drops are disintegrated. If the incoming droplets are smaller than the wire, they have a tendency to form a thin liquid film which exists consistently on the wire. This film accumulates and wraps around the wire from both sides. It forms a liquid ligament at the bottom side of the wire. This ligament continues to grow in the form of a pendant drop. Eventually, when the weight of the pendant drop is large enough to overcome the surface tension force associated with the contact surface of the wire, the drop detaches from the wire. A new correlation for the size of the dripping drops with non-dimensional wire Bond number has been derived.

4.1 Regular Droplet Impaction

Figure 4.1 displays the schematic of the droplets impacting on wire at regular offset. The wire was located at about 10 cm below the nozzle and was bent into a L-shape. The viewing direction of the camera was taken from the end along the wire. In the study, the excitation frequency of the piezoelectric transducer was set at 1000 Hz, which was also the collision rate of the droplets with the wire. The mono-size droplet stream with diameter of 680 μm at an incoming velocity about 2.0 m/s was produced. The uniform spacing between the centers of two droplets is approximately three times of the droplet diameter. Under this condition, 5 wires with various diameters were studied for the impaction: 381, 508, 813, 1190, and 1588 μm. For each wire, the droplets were impacting at different offsets relative to the wire.

Figure 4.1 Schematic of regular offset droplet impaction

4.1.1 Non-dimensional Parameters

The controlling parameters of the impacting phenomena in this study are the incoming droplet diameter (d) , droplet velocity (V_o), fluid property of the droplet (ρ_l, σ), wire diameter (D), and the offset distance of the incoming droplet relative to the wire (δ). A more generalized representation of these parameters can be grouped into non-dimensional form, namely, the droplet Weber number (*We*), the offset ratio of droplet relative to wire (Δ), and the ratio of incoming droplet diameter to the wire diameter (*R*) with the following definitions:

$$We = \frac{\rho V_o^2}{(\sigma/d)} \tag{4.1}$$

$$\Delta = \frac{\delta}{(d+D)/2} \tag{4.2}$$

$$R = \frac{d}{D} \tag{4.3}$$

where the Weber number is the ratio of inertia force to the surface tension. With the above definitions, the values for the controlling parameters in this study were as follows: The droplet Weber number was found to be 37.9. The drop diameter to wire diameter ratio was between 0.43 and 1.77. Note that the offset value δ can be measured from either side of the wire. The offset ratio Δ was between 0.0 and 1.0. No contact between the droplet and wire was made if the offset ratio was larger than 1.0.

This study is the first attempt to investigate the impacting process on cylindrical wires using a single droplet stream. The size of the droplets is selected for experimental convenience.

4.1.2 Results and Discussions

Generally, the impacting phenomena include the stages of attachment, accumulation of liquid film, and the detachment. Various offsets of the incoming droplets with respect to the wire and the ratio of droplet size to wire size affect the outcome of impaction substantially. When the liquid droplet impacts the convex surface, as in our present case, a water film spreads onto the wire. The surface of the wire becomes wetted. This film runs off from the point of contact and forms an elongated water ligament beneath the wire. Larger drops are generated from the detachment of this ligament. The results discussed here are limited to the present experimental conditions being studied.

Figure 4.2 shows the pictures of a water droplet stream, 680 μm in diameter, impacting on the smallest wire with diameter of 381 μm (R = 1.77). The droplets approach the wire at the right side. At large offset with Δ equal 0.95, the droplets slightly touch the wire and the contacts do not affect the shape of the droplets significantly. The droplets departing the wire are distorted slightly; however, the spacing between the droplets and their velocity are about the same as before the impact. At a smaller offset of 0.63, a portion of each droplet is in direct contact with the wire, and a small fluid ligament builds up from the point of contact. It can be seen that the droplets are further distorted and become more irregular in shape. The droplets remain moving vertically downward at about the original size and velocity. At a near head on collision with very small offset of 0.11, the droplets hit the wire directly from above. Since the droplets are larger than the wire, the liquid wraps around the wire in both directions from the point of contact. The films then regroup at the bottom of the wire to form an elongated ligament of liquid. As this ligament becomes longer, drops are formed by detaching from the end of this ligament and drip off downward. It can be seen that the droplets generated below the wire are slightly larger than the ones before the impact and possibly at a slower velocity.

The phenomena of impacting droplets on a larger wire with diameter of 813 μm (R = 0.83) are displayed in Fig. 4.3. In this case, the wire is slightly larger than the droplets. When the droplets barely touch the wire at a large offset Δ of 0.92, the behavior resembles to the previous case of large offset. The contacts do not change very much the outcome of the droplets' spacing, size, or velocity. However, when the droplets approach more towards the center of the wire from above, at an offset of 0.33, a thicker liquid film builds up from the side of contact due to droplet coalescence. There is a also much longer and thicker fluid ligament attached from the bottom of the wire. This shape of the ligament becomes very irregular and wriggles around. The wriggling of the ligament also induces agitation. When the ligament becomes long enough, a new drop is formed by liquid detachment from the end of this ligament. This droplet is much larger than the original droplet. At a very small offset of 0.09, a very large and nearly spherical drop of about 5.1 mm in diameter is formed, prior to detaching from the wire.

Similar phenomena can be found in Fig. 4.4 for the case of droplets impacting on the largest wire with diameter of 1580 μm (R = 0.43). At a large offset Δ of 0.93, the droplets slightly touch the wire and the contacts have a negligible influence on the spacing, velocity, and shape of the droplets. At a medium offset of 0.59, as shown in this figure, the accumulation of the liquid droplets in a form of liquid film builds up a even thicker ligament beneath the wire. Like the previous case, the wriggling of this ligament causes agitation and induces a detachment of a large drop from the bottom of the ligament. However, at a small offset of 0.05, this ligament does not wriggle very much. It starts to neck and a huge drop of about 6.5 mm is slowly formed. Eventually, the weight of the drop becomes sufficient to induce detachment from the ligament beneath the wire.

Figure 4.2 Impacting phenomena of droplets on 381 μm wire (R = 1.77)

Figure 4.3 Impacting phenomena of droplets on 813 μm wire (R = 0.83)

Figure 4.4 Impacting phenomena of droplets on 1588 μm wire (R = 0.43)

The cases with wires of 508 μm (R = 1.32) and 1190 μm (R = 0.57) in diameter exhibit trends similar to the three extreme cases described above. To summarize the outcomes of all the impacting phenomena in this study, a regime map is provided in Fig. 4.5. This map is plotted based on the non-dimensional parameters of the offset ratio (Δ) and the wire to drop diameter ratio (R^{-1})at the Weber number of 37.9. For large offsets, single drops at similar size and velocity are generally found independent of the variation of the drop to wire size ratio. For medium and small offsets, liquid film builds up on the wire and generates a ligament. Larger drops are formed as a result of detachment from the end of the ligament. If

the drop is much smaller than the wire, then even larger drops are generated. The boundaries of the zones in this map are not sharp; however, they serve as a first order estimation of the outcome of other similar impacting processes. Smaller droplets, for example, may have a different impact behavior because of the higher surface forces. In addition, the phenomena of water spreading on the wire may be dependent upon the fact that a water film exists consistently on wire. Therefore, it is expected that the boundaries of the zones could be slightly different at other Weber numbers and/or droplet impaction rates.

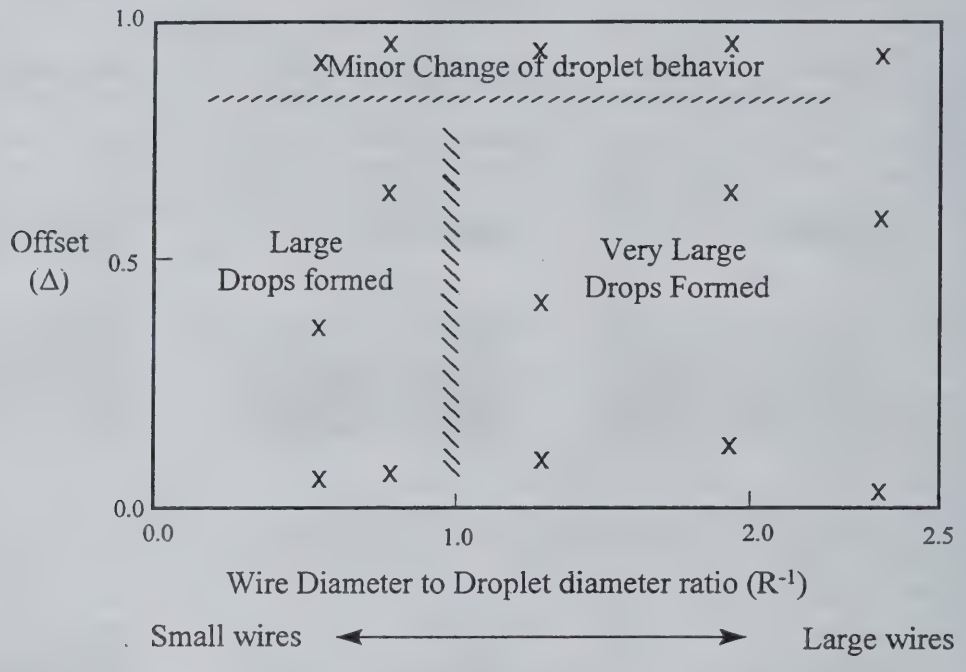

Figure 4.5 Regime map for the outcome of regular offset impaction (We = 37.9, droplet diameter = 680 μm, droplet rate = 1000/sec)

4.2 Single Droplet Impaction by Drop-On-Demand Condition

Figure 4.6 shows the dripping drops phenomena of another situation of droplet impaction on wires. In this case, the droplets are generated using a modified droplet generator through a drop-on-demand operating condition. The droplets are approximately 110 μm in diameter moving downward at about 1 m/s. They impact on the wires directly without the influence of the air jets. The droplet Weber number is about 4.0. At such a low Weber number condition, the droplet has very little inertial force and the interfacial contact is dominated by the surface tension effect. As shown in Fig. 4.6, the profile of the hanging drops highly resembles the pendant drop situation. This suggests that the dripping phenomena will be a purely gravity induced situation. In general, the dripping drops are larger as the wire size increases, due to a larger interfacial contact area. Once the volume of the pendant drop reaches a critical value, necking begins near the contact point and the drop detaches from the wire.

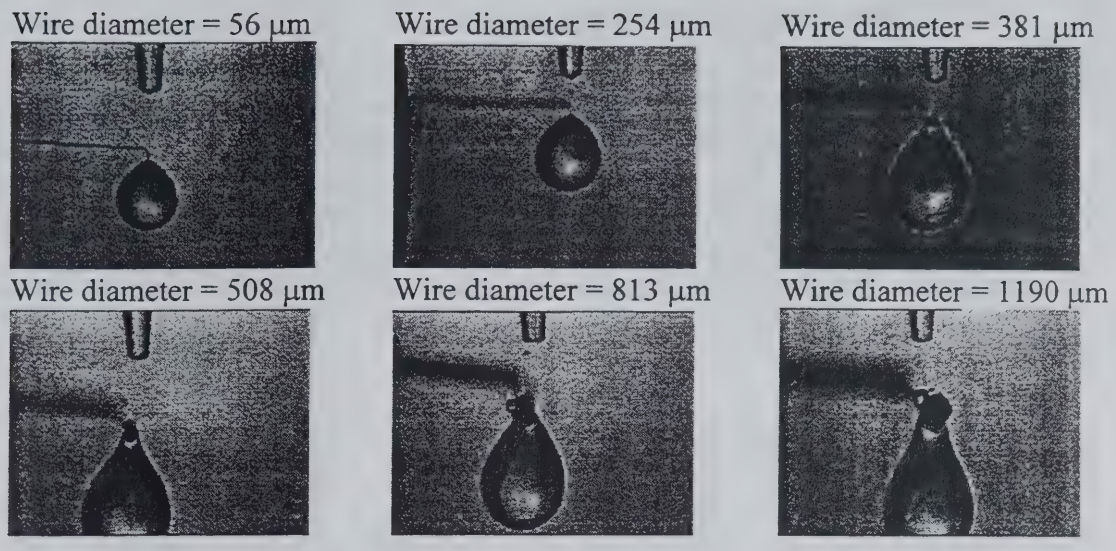

Figure 4.6 Phenomena of droplets hanging on wires (Drop-on-demand mode) (Droplet Weber Number = 4, droplet diameter = 110 μm)

4.3 Random Droplet Impaction

Figure 4.7 illustrates another experimental study of the droplets impacting on wire at random offset. Mono-size water droplets of 350 μm in diameter were generated using the droplet stream generator. The droplet stream was then perturbed by two small opposing air jets so that the droplets became more randomly spread when they approached the wire. The velocity of the droplet was determined by measuring the jet diameter and the volume flux which gave the incoming velocity ranging between 2.8 m/s and 7.0 m/s. Four velocities of the droplets were used for the impaction studies which corresponded to the droplet Weber number conditions of 41, 98, 172, and 230. Seven wires of various sizes were selected in the present investigation: 113, 254, 381, 508, 813, 1190, and 1588 μm. The volumetric flux was determined by direct collection of local flux at the location where the wire was located. It was measured to be 17.6 cc/min/cm^2.

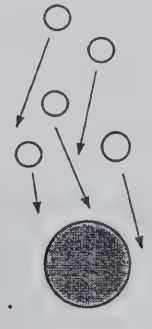

Figure 4.7 Schematic of random offset droplet impaction

4.3.1 Non-dimensional Parameters

The controlling parameters of the impacting phenomena in this part of study are the incoming droplet diameter (d), fluid property of the droplet (σ, ρ_l), incoming droplet velocity (V_o), and the wire diameter (D). In addition, dripping drop may be formed gradually beneath the wire under the influence of gravity in some cases. Therefore, the gravitational constant (g) and the size of the dripping drop (D') are also considered in the analysis. Figure 4.8 shows the schematic drawing of the impacting situation.

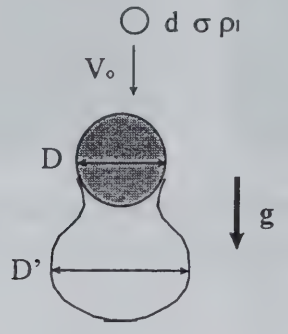

Figure 4.8 Physical parameters for the impacting situation

A more generalized representation of these parameters can be grouped into four non-dimensional forms. In addition to the droplet Weber number (*We*) and the size ratio of wire diameter to the incoming droplet diameter (*R*), the size ratio of the dripping drop to the wire diameter (*R'*) and the Wire Bond number (*B*) are also employed in this analysis with the following definitions:

$$R' = \frac{D'}{D} \tag{4.4}$$

$$B = \frac{D}{\sqrt{(\sigma / g\rho_l)}} \tag{4.5}$$

The wire Bond number is the ratio of the gravitational force to surface tension. This Bond number is important in the analysis when the effect of gravity is considered for the drops dripping under the wire.

4.3.2 The Random Droplet Impaction Phenomena

Generally, when the droplets impact on the wire, they have a tendency to wet and stick to the surface. The contact usually creates a thin liquid film on the wire. Depending on the size of the wire, this thin film may either break up into smaller drops if the wire is small, or it may grow into a ligament hanging beneath the wire if the wire is large. This ligament may evolve into a wriggling fragment or a pendant drop profile which eventually would detach from the wire. Figure 4.9 shows the typical classifications of the droplet impacting phenomena on wires, which are the disintegration mode, momentum-induced dripping mode, and gravity-induced dripping mode.

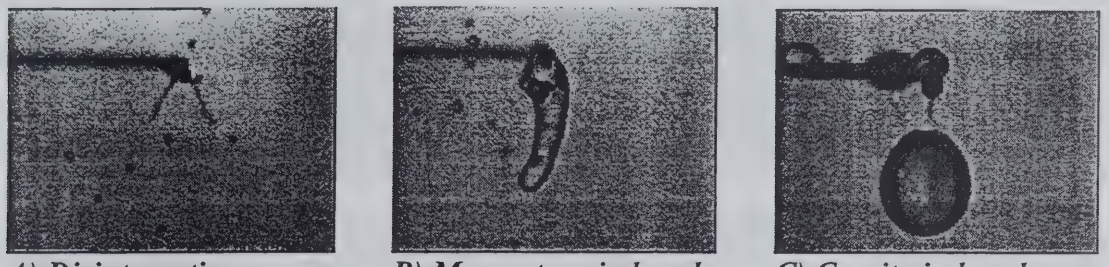

A) Disintegration *B) Momentum-induced dripping* *C) Gravity-induced dripping*

Figure 4.9 Typical classifications of the droplet impacting phenomena

The disintegration mode occurs primarily when the droplets of moderate impacting velocity come into contact with a wire which is smaller than the incoming droplet. If the droplet velocity is very high, this mode would also happen even if the wire is larger than the droplet. As shown in Fig. 4.9A, when the droplets impact onto the surface of the wire, the wire serves as a shearing or cutting medium to the droplet. The minimal contact between the droplets and the wire causes a small surface tension effect at the interface. The water film being developed on the wire warps around the top portion of the wire and forms a 'V' shaped fragment. It splits into two halves, one on each side. Each small fragment behaves like a small water jet and emerges straightly outward. Eventually, each thin liquid jet disintegrates into even smaller drops.

Figures 4.9B and 4.9C demonstrate the phenomena of drops dripping from the bottom of the wire. This observation can be divided into 2 modes: (1) momentum induced dripping mode, and (2) gravity induced dripping mode. These modes are usually observed when the wire is larger than the droplet size. The gravity induced dripping resembles to the situation of dropwise condensation from the bottom of the horizontal tubes.

In the momentum induced dripping mode, when the incoming droplets make contacts with the wire, a water film builds up consistently. The film runs off from the contact point and wraps around the wire from both sides, and finally the film reattaches and forms a large fragment beneath the wire. There are two reasons for which a longer and thicker fragment is formed. Firstly, the water film carries downward momentum from the top side of the wire,

and secondly, droplets may impact on this ligament directly without hitting the wire. The shape of this fragment is very irregular. As the fragment becomes larger, it wriggles more vigorously under the influence of gravity as well as the momentum added by the impacting droplets. Finally, the surface tension at the interfacial contact can no longer sustain the combined effect of the weight and the downwards force of the impacting drops on the ligament. At this point, the drop detaches from the wire and drips off.

In the gravity induced dripping mode, the formation process of the dripping drops is very similar to the previous case. However, the shape of the dripping drops are much more spherical. The liquid feeding into the ligament carries less downward momentum due to larger size of the wire or lower droplet velocities. As a result, the shape of the ligament resembles to the form of a pendant drop. Eventually, when its weight is large enough to overcome the surface tension at the wire interfacial surface, the drop detaches from the wire and drips off at gravity. The size of the dripping drops in this case is usually larger than the ones in the case of momentum induced dripping. Occasionally, there are some satellite drops formed when the big pendant drop detaches from the wire.

Figure 4.10 shows the typical impacting phenomena as a function of wire size from 113 to 1588 μm and the droplet Weber number from 41 to 230. The incoming droplet size is 350 μm for all these cases. Disintegration occurs consistently when the droplets impact on the 113 μm wire (R = 0.34), regardless of the Weber number condition. For a larger wire diameter of 254 μm, disintegration only occurs at the higher Weber numbers of 172 and 230. For even larger wires of 381 μm and 508 μm, disintegration only appears at the highest Weber number of 230. At the wire size of 813 μm and larger, no more droplet disintegration is observed.

Phenomena of momentum induced dripping also occur in a limited range of droplet Weber number and wire size. At the lowest Weber number of 41, all the dripping drops tend to be gravity-induced. At the Weber number of 97, droplets impacting on wires with diameter of 254, 381, and 508 μm give rise to momentum induced dripping drops. At a higher Weber number of 172, similar phenomena also occur at larger wire sizes of 381 μm and 508 μm. As the Weber number further increases to 230, only the wire of 813 μm would result in a momentum induced dripping phenomena. All other cases of droplets dripping from the wires show a reasonably spherical form of the pendant drops, indicating the situation of gravity induced dripping mode.

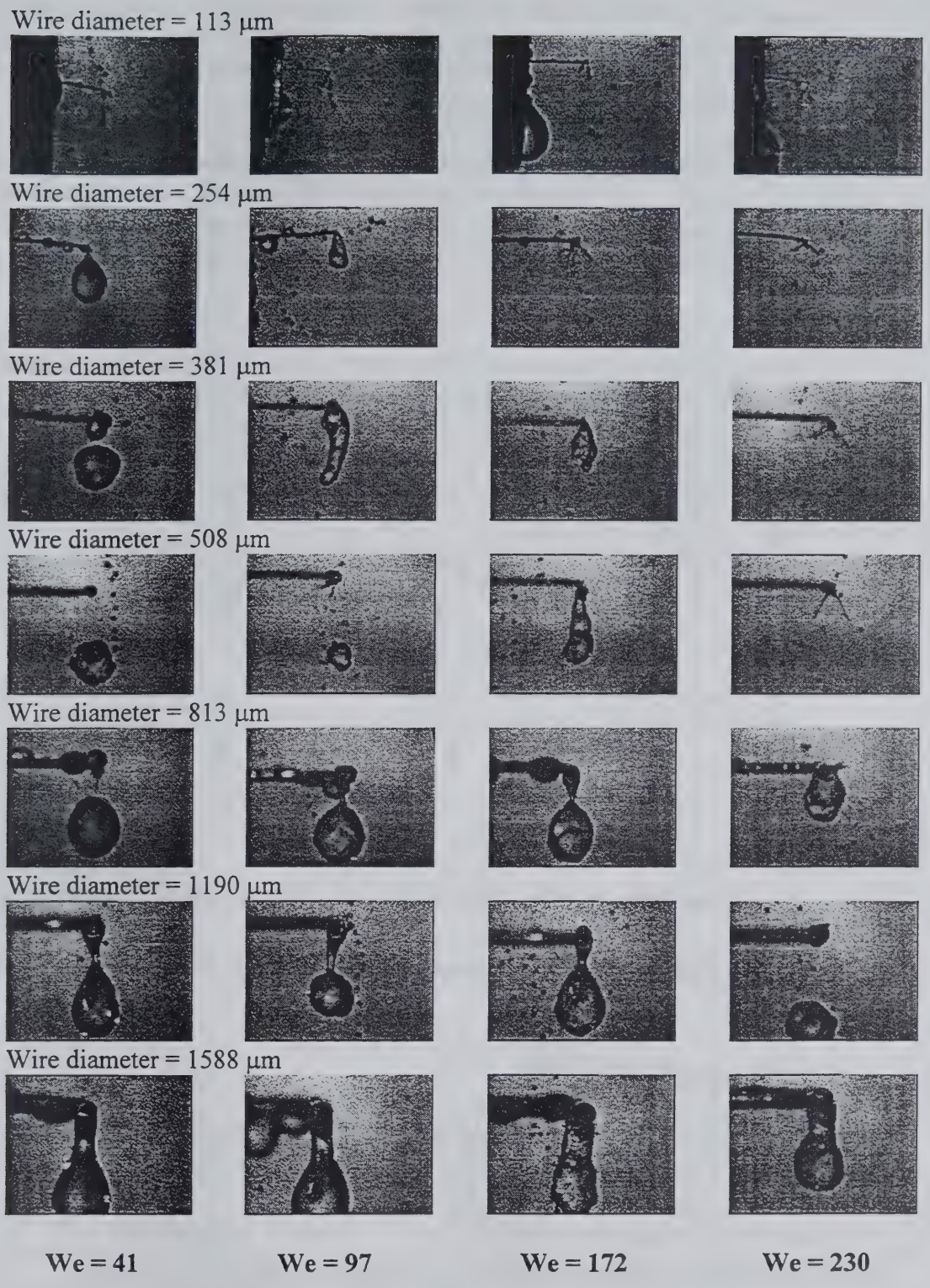

Figure 4.10 ***Phenomena of random droplets impacting on wires (Incoming droplet diameter = 350 μm)***

To summarize all the conditions studied, a regime map is obtained to provide an overall quantitative analysis for the outcome of the impacting process. This is presented non-dimensionally in terms of the incoming droplet Weber number (We) and the size ratio of wire diameter to droplet diameter (R). This regime map is displayed in Figure 4.11.

On the regime map, the square symbols represent the disintegration mode (Regime I), the triangle symbols are for the momentum induced dripping mode (Regime II), and the circle symbols are for the gravity induced dripping mode (Regime III). Two lines are used to divide the different regimes. The boundaries of the zones in the map are not sharp, but they can be used as a first order criteria for predicting the impacting outcome of other similar process.

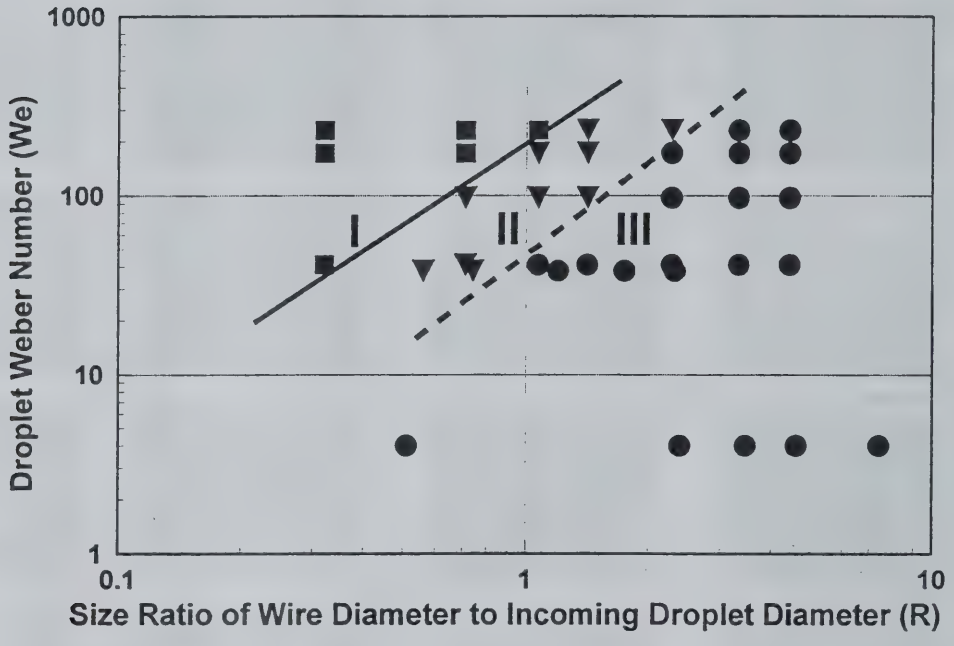

Figure 4.11 ***Regime map of the overall impacting phenomena***

4.4 The Dripping Drops

As reported earlier, dripping drops are frequently observed due to the formation of the liquid fragment under the wire. It is therefore of interest to quantify the size of the dripping drops as a function of the wire size and Weber number.

From the photographs shown in Fig. 4.9, it can be observed that some of the dripping drops are not truly spherical. After detaching from the wire, they appear to be the prolate spheroids with a major axis L_1 and a minor axis L_2. An equivalent drop diameter of a prolate spheroid can be found by equating its volume in the following equation:

$$\frac{4}{3}\pi\left(\frac{L_1}{2}\right)\left(\frac{L_2}{2}\right)^2 = \frac{1}{6}\pi(D')^3 \tag{4.6}$$

Therefore, the equivalent diameter of the dripping drop can be found by:

$$D' = \sqrt[3]{L_1 L_2^2} \tag{4.7}$$

This formulation is used for deducing the data from non-spherical dripping drops.

Figure 4.12 shows the relationship between the diameter of the dripping drops and the wire size at three Weber numbers of 41, 97, and 230. The typical size range of the dripping drops is between 2.6 mm and 4.4 mm. In general, a larger dripping drop is associated with a larger wire at a given Weber number condition. The rate of increase gets smaller as the wire size increases. However, as the Weber number increases, the droplets give more downward momentum in addition to the weight of hanging drop to balance with the surface tension. This gives a smaller size of the dripping drops.

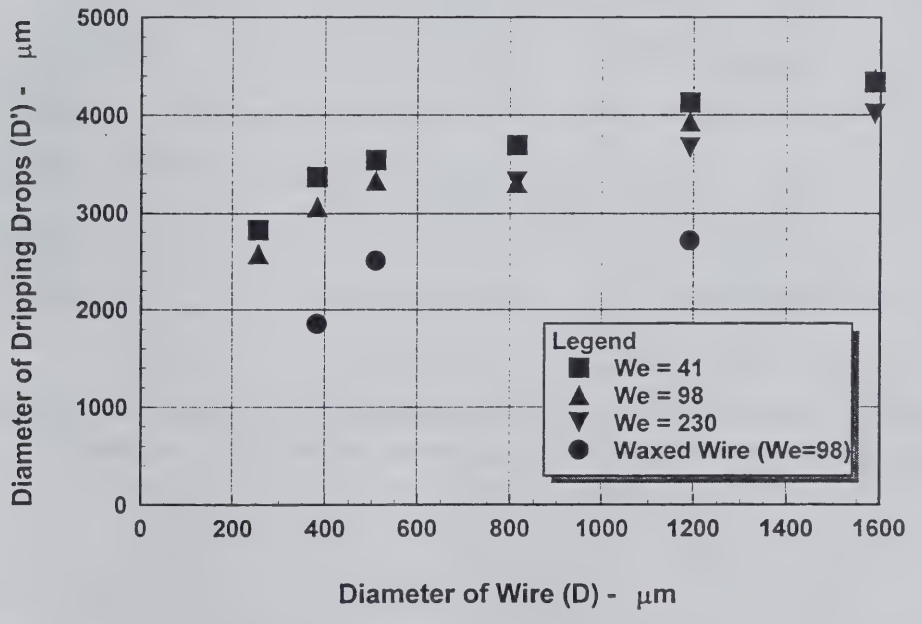

Figure 4.12 Plot of size of dripping drop verses wire diameter

4.5 Droplets Impacting on Waxed Wires

The wetting effect of the surface would affect the interfacial contact and the contact angle between the liquid phase and the solid surface. Consequently, it would influence the size of the dripping drops. Therefore, a preliminary investigation of the droplets impacting on waxed wires has also been studied. The dripping size of the drops is estimated from the images. As shown in Figure 4.12, at the Weber number of 98 and for the wire diameters of 381, 508, and 1190 μm, the dripping drops detached from the waxed wires are about 40% smaller than the ones from the non-waxed wires. This is because when the surface of the wire is waxed, the interfacial contact angle between the wire and the liquid film increases and the effect of surface tension is reduced. Therefore, the film has much less tendency to stick or wet the waxed surfaces. Similar observations have also been found on another impaction study in which the droplets impacted onto the non-wetting Teflon wire.

Figure 4.13 displays a log-log plot of the size ratio of the dripping drop to the wire diameter (R') verses the wire Bond number (Bw). The wire Bond number is an important parameter for the dripping drop measurement because it relates the balance of surface tension with the gravitational effect. All symbols generally fall onto linear trends on the log-log plot. It appears that the trend is relatively independent of the Weber number condition. Using a least square fit method to fit the available data, the correlation for the non-waxed wire is found to be:

$$R' = 1.813 B_w^{-0.786} \qquad (4.8)$$

And for the waxed wire impaction at the Weber number of 98, the correlation is:

$$R' = 1.299 B_w^{-0.722} \qquad (4.9)$$

Within the experimental range, Equations (4.8) and (4.9) can be used to predict the size of the dripping drops at any given Bond number with a reasonable confidence.

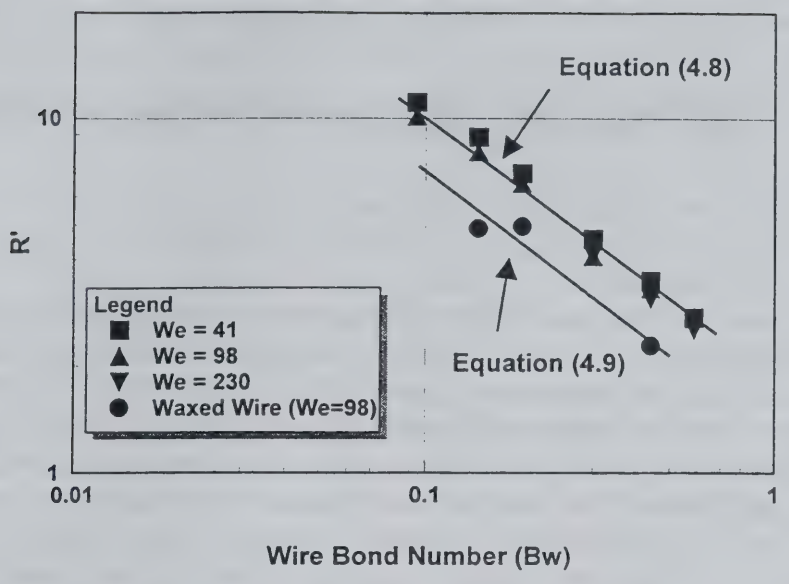

Figure 4.13 Plot of R' verses Wire Bond Number (B_w)

4.6 Concluding Remarks

Experimental studies of water droplets impacting on cylindrical wires were conducted systematically. The effect of droplet velocity and the wire sizes were varied parametrically to reveal the impaction characteristics. The operation of the two droplet generators showed high potential for generating droplets in a variety of operating conditions. Some concluding remarks of the investigation are listed below:

1) The typical modes of impaction outcome were disintegration and dripping. Smaller droplets were disintegrated if the incoming droplets had higher velocity or the wire diameter was small. Larger dripping drops were formed when the velocity was low or the wire diameter was large.
2) A non-dimensional map was obtained to identify the regime of disintegration mode, the momentum induced dripping mode, and the gravity induced dripping mode. This map could be used to predict the impacting outcome at similar conditions.
3) The sizes of the dripping drops were measured and were plotted against the wire Bond number. The non-dimensional dripping size had also been correlated well with the Bond number. A linear trend on a log-log plot exhibited that the wire Bond number was an important parameter for dripping drop size measurement.
4) The contact angle effect was also examined by studying the droplets impacting on waxed wire. The drops dripping from waxed wires were generally smaller than the ones from the non-waxed wires due to the reduced surface tension effect at the interfacial contact.
5) Results of regular offset impaction and drop-on-demand impaction were consistent with the random offset impaction situations.

Chapter Five

The Impaction of Droplets on Horizontal Screens

Summary

This chapter presents the continuation of the droplet impaction experiments on wire screens. Mono-size droplets of 350 μm in diameter were generated using a piezoelectric droplet generator. For droplets impacting on coarse screens, they wetted the wires by forming thin liquid lumps. As these lumps of water film accumulated around the wires, dripping drops were produced on the bottom side of the wire. This phenomenon was very similar to the dripping drops from a single wire situation presented in previous chapter. For finer screens, the liquid film on the top surface permeated through the fine mesh openings and formed liquid ligaments at the bottom side of the screen. This ligament continued to grow in the form of a pendant drop. This situation resembled a dripping phenomenon from the bottom side of a flat surface. Eventually, when the weight of the pendant drop was large enough to overcome the surface tension effect associated with the contact surface of the screen, the drop detached from the wire and dripped off.

5.1 Background

The penetration of droplets through the screen structures is widely encountered in a variety of industrial applications. For example, in distillation processes, woven wire screens are used extensively for separating the liquid droplets from gaseous streams. They can also be utilized in typical process plants for size classification, product separation, impurity removal, particle filtration, and mist elimination (Muldoon, 1984; Capps, 1994). In addition, ventilating screens are often employed in electronic equipment compartments. In order to extinguish the fire which occurs inside the compartments, fine water mist flow can be applied to penetrate into the compartments through these ventilating screens. Hence, the interactions of the mist droplets with the screen are essential for the fire suppression effectiveness.

A typical mesh screen is made up of wires of a particular diameter interweaving together to form a perforated planar structure with a desirable mesh opening size. Depending on the applications, the wire sizes and mesh openings of a screen may vary typically from micrometers to millimeters. The texture of the woven wire screen may be as soft and flexible as silk cloth or as rigid and durable as solid steel plate (Soar, 1991).

When droplets carried by gaseous streams pass through a screen, some droplets may be trapped by the wire meshes while others may penetrate through directly. Even though the screens may appear to be planar in many practical applications, their characteristics subject to droplet impaction are far more complicated. During the impaction, thin liquid films may build up on both sides of the screens. In Chapters Two, it has been demonstrated that the penetration of droplets is dependent upon the blockage fraction (B) of the object's configuration. Therefore, once these films evolve into the dripping drops under the screen,

they would obstruct partially the clear flow path of the original mesh opening configuration and alter the blockage fraction (i.e., B) of the mesh screens. As a result, the overall penetration processes are strongly influenced by the droplet size, the flow condition, the configuration of the screens, and the behavior of the liquid films subsequent to the impaction process.

Much of the available literature on the droplet impacting phenomena is only applicable to flat solid surfaces (Chandra and Avedisian, 1991; Cohen, 1991; Fukai, et al., 1995). However, the impacting phenomena of the droplets on wire screens remain uncertain because very limited literature in this area has been reported. Apart from the results of the penetration of sub-micron range ultrafine particles through fine screens (Wang, 1996; Ichitsubo et al. 1996), not much information is available for larger droplets impacting on screens with wires of comparable sizes. Therefore, the objective of this study is to investigate the phenomena of water droplets impacting on wire screen structures. Figure 5.1 displays the schematic of the impacting process. Since a wire screen is composed of a multitude of interweaving wires, the fundamental understanding of droplets impacting on single wires (Hung and Yao, 1997) will provide an essential basis for the impacting process on more complex wire screen structures.

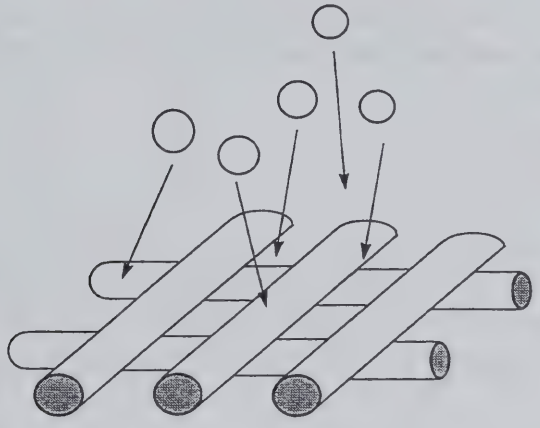

Figure 5.1 Schematic of the droplets impacting on a horizontal screen

5.2 Description of the Wire Mesh Screens

Some common types and general specifications of wire screens have been reviewed by Muldoon (1984). Plain square weave wire screen was chosen for the current investigation. The square meshes are formed by passing wires over and under other successive warp wires in a perpendicular orientation. The term 'mesh' refers to the number of openings per linear inch. The distance is the length between the two centers of the adjacent parallel wires, which is simply the inverse of the mesh number. The clear width of mesh opening is the distance minus the diameter of the wire. For example, a 5 by 5 mesh screen with diameter of 0.063 in (1.588 mm) has 5 square openings per inch on each side, a distance of 0.2 in (5.08 mm)

between the diameters of the 2 wires, and a clear width of mesh opening of 0.137 in (3.48 mm).

In the current experiments, 20 plain weave, stainless steel screens with different wire sizes and mesh openings were selected. They were supplied from several commercial screen manufacturers. The dimensions of the screens were ranging from a coarse screen of 1.6 mm wire diameter with 2 by 2 meshes to a fine screen of 0.14 mm wire diameter with 100 by 100 meshes.

5.3 Results and Discussions

5.3.1 The Impaction Phenomena

Experimental results show that some droplets may pass through the meshes of certain coarser screens without hitting them. As the screens become finer, some droplets may impact on the screens directly. These droplets tend to wet the wires and create thin liquid films (Padday, 1957). Figure 5.2 displays the schematic of the general behavior of the droplets impacting on a horizontal screen. Thin liquid films can be accumulated randomly over the screen surface. As the liquid films build up, they warp around the wires which cause dripping drops on the bottom side of the screen.

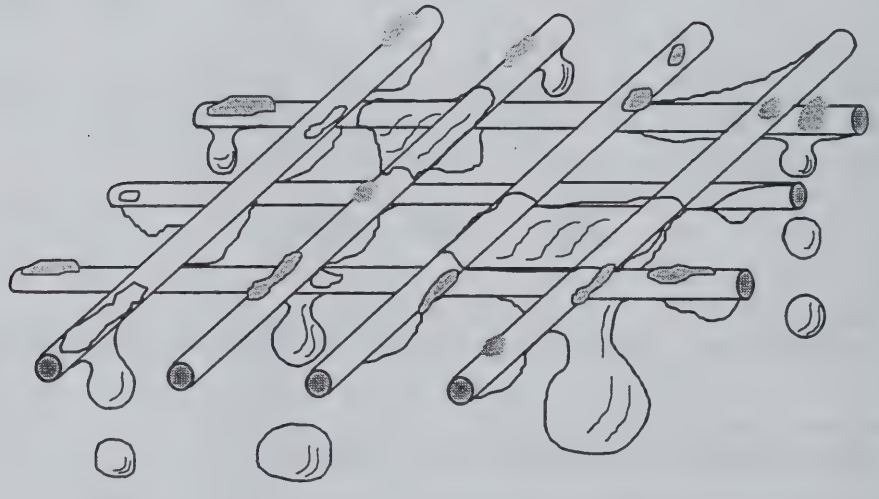

Figure 5.2 General impacting phenomena of droplets on a horizontal screen

For all the screens being studied, the dominant outcome of the impaction is the dripping phenomena. The specific dripping characteristics depend on the incoming droplet size, velocity, the wire diameter of the screen, and the size of the mesh opening. Typically, large dripping drops are formed at different locations across the screen, for example, at the bottom side of a single wire, at the corners of the meshes, and even at the mesh stitch apertures surrounded by the wires. If the screen is very fine, the accumulation of droplets would form a thicker film on top which gradually permeates to the bottom side. The pendant drops

forming in this situation resembles a flat plate dripping situation. The overall dripping drop formation can be approximately divided into 4 types of dripping observations. It is noted that different dripping phenomena can be observed simultaneously in a given screen. The identification for differentiating the various observations is based on the dominant outcome of the phenomena.

Droplets with higher impacting velocity of about 7 m/s were also tested for the impaction study. However, it was found that the droplet velocity of 7 m/s did not affect the impacting phenomena substantially.

5.3.2 Dripping Drops Formed under Single Wires (Type 1 and Type 2)

Figure 5.3 displays both the top and bottom viewing perspectives of the phenomena of droplets impacting on a coarse screen of 2 x 2 mesh with wire diameter of 1.19 mm and a clear width of mesh opening of 11.51 mm. In general, during impaction, lumps of water wet the wire surface and stick onto the wire at the locations of the impact. The liquid film gradually warps around the wire as more droplets accumulate. As seen in the pictures, some drops are hanging under the bottom side of the wire. The film gradually evolves into a pendant drop profile. Eventually, the weight of each drop becomes large enough to overcome the surface tension force at the interfacial contact and the drops detach from the wire and fall down. This dripping phenomenon resembles the situation of that for a single wire (Hung and Yao, 1998). In addition to the main dripping drops, smaller satellite droplets are occasionally formed after the primary drops detach from the screen. In addition, dripping drops also occur at the corners of the meshes formed between 2 crossing wires. The dripping drops formed at these locations are generally larger than the ones formed at the bottom side of a single wire. This is because the interfacial contact area between the liquid and wire at the corner locations is larger than that at the bottom side of a wire, creating a larger surface tension force.

5.3.3 Dripping Drops Formed under Single Mesh Aperture (Type 3)

Dripping also occurs under single mesh apertures surrounded by the wires, as demonstrated in Figure 5.4 for a medium screen of 8 x 8 meshes with wire diameter of 0.71 mm and a clear width of mesh opening of 2.46 mm. This screen is finer than the previous one. In accordance with the observation by Padday (1957), the droplets that coalesce the wires will reach a critical volume when spreading to form a film over the surface. The film is then drained toward the 'cross-over' points of wire in the basic interweaving structure. There are the locations where the effective pore apertures are smallest (Feord et al., 1993). As displayed in the pictures, instead of dripping directly under the wires as in the previous situation, pendant drops are formed mostly under the mesh stitch apertures. The size of the pendant drops can be determined by the physical dimensions of the aperture which is dependent on the stitch geometry of the woven screen. Generally, the dripping drops in this case are larger than the ones in the pervious case.

5.3.4 Dripping Drops Formed under a 'Flat' Surface (Type 4)

Figure 5.5 displays another situation of droplets impacting on a very fine screen. This screen has 60 x 60 meshes with wire diameter of 0.19 mm and a clear width of mesh opening of 0.23mm. This fine screen resembles a perforated flat sheet with miniature mesh openings. For droplet impacting on a fine screen, a thin water film is generally built up on the top side of the screen. This film becomes thicker and it gradually permeates to the bottom side through the tiny mesh openings. This film continues to grow underneath in the form of a pendant drop under the gravity effect. This situation resembles the breakaway of a drop from a flat horizontal wetted surface (Tamada and Shiback, 1966). As demonstrated in Fig. 5.5, there are 3 potential spots where the dripping drops are forming. Eventually when the weight of the pendant drop is large enough to overcome the surface tension force associated with the contact area of the screen, the drops break away by detaching from the screen.

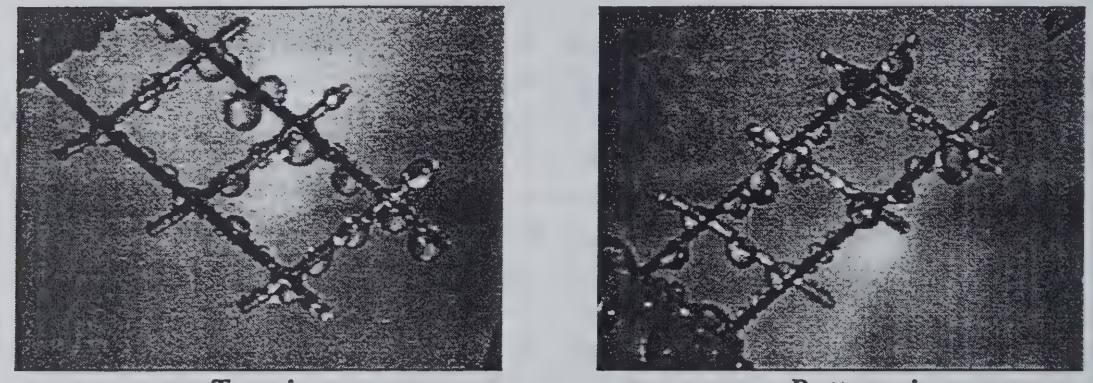

Top view *Bottom view*

Figure 5.3 2 x 2 mesh screen with wire diameter of 1.19 mm

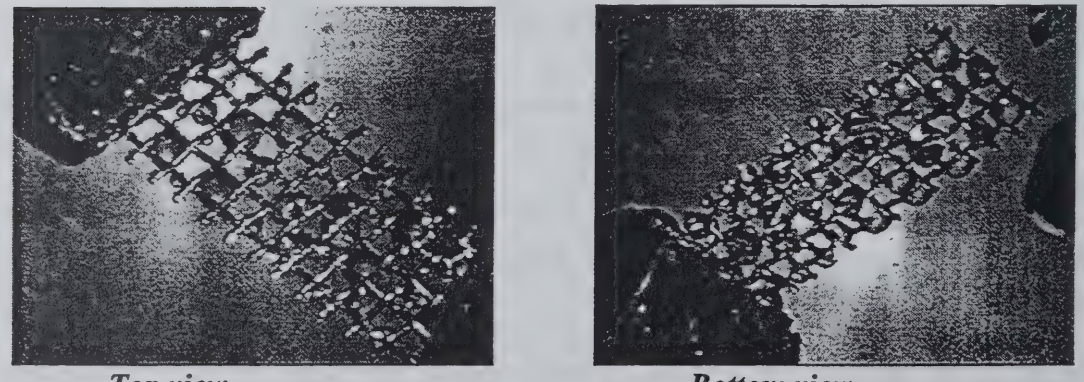

Top view *Bottom view*

Figure 5.4 8 x 8 mesh screen with wire diameter of 0.71 mm

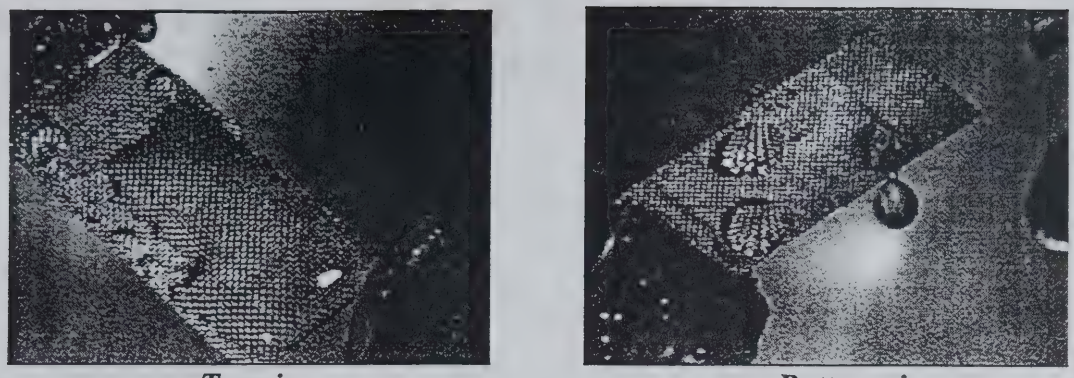

Top view *Bottom view*

Figure 5.5 60 x 60 mesh screen with wire diameter of 0.19 mm

5.4 Non-dimensional Parameters

Non-dimensional parameters and correlations will be used to analyze the outcome of the impaction characteristics. The controlling parameters of the impacting phenomena in this study are the incoming droplet diameter (d), fluid property of the droplet (σ, ρ_L), incoming droplet velocity (V_o), the wire diameter (D), and the clear width of mesh opening (L).

A Screen parameter (S) is used to describe the type of screen with the following definition (Cheng and Yeh, 1980):

$$S = \frac{4\beta h}{\pi(1-\beta)D} \tag{5.1}$$

In our screen selection, the wire diameter (D) and the screen thickness (h) are assumed to be of the same size. The β is the solid fraction of the screen which is a function of both L and D. In general, a fine screen is represented by a high S value.

Figure 5.6 displays a regime map for the different types of dripping drop formations on a screen by plotting the clear width opening non-dimensionalized by the incoming droplet diameter against the screen parameter. Dripping drops are usually observed either from the underside of the wires or from the mesh stitch apertures. Type 1 (solid square symbols) represents the dripping drops formed at the bottom side of a single wire while Type 2 (solid circle symbols) represents those formed at the corners of the meshes. Type 3 (open square symbols) is for the dripping drops formed under the mesh apertures and Type 4 (open circle symbols) resembles the drops dripping off from a flat horizontal surface. A dotted line is drawn on the map to globally identify the primary dripping drop formation. Typically, dripping drops formed under wires or corners are associated with coarser screens which are to the left side of the line. On the other hand, dripping from meshes is likely to occur for finer screens on the right side of the line. This dotted line only serves as a first order prediction for

the outcome of similar impacting processes. It is believed that the line could be drawn slightly different at other incoming droplet sizes, velocity, and volumetric flux.

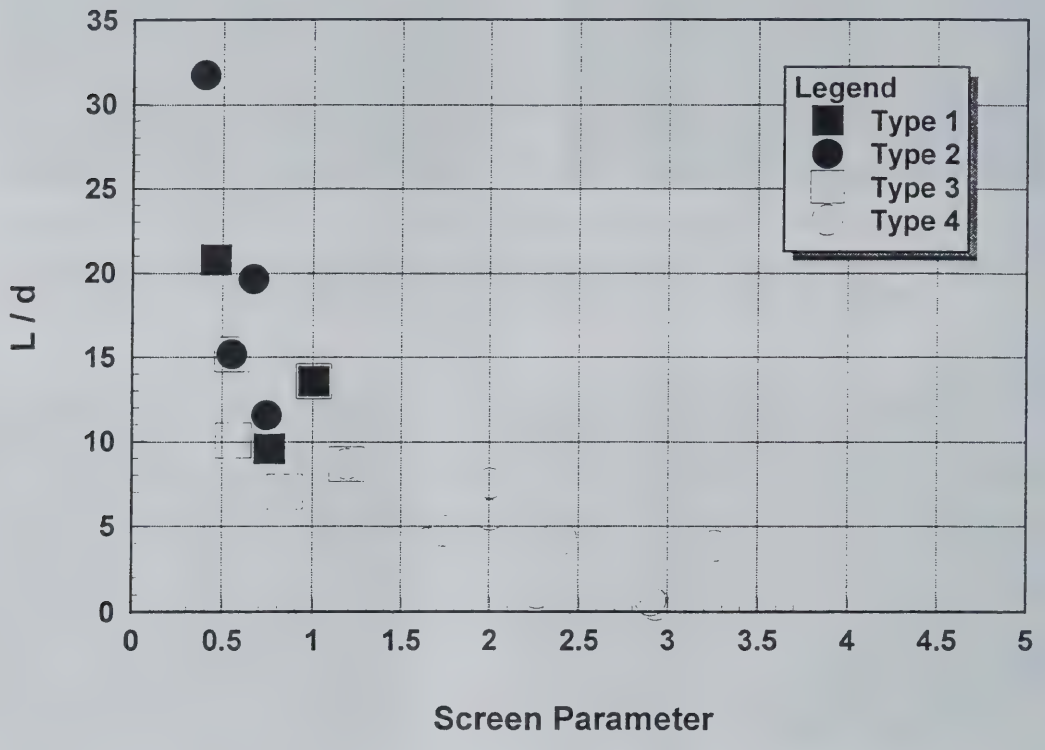

Figure 5.6 A regime map for the phenomena of dripping drops from screens

5.5 Measurement of the Size of the Dripping Drops

It is observed from the images that some of the dripping drops may not be truly spherical, but look similar to the prolate spheroids. Therefore, an equivalent drop diameter of a prolate spheroid can be found by using the equations 4.6 and 4.7 outlined in the previous chapter to deduce the corresponding diameter of the dripping drop.

Figure 5.7 illustrates the relationship between the diameter of the dripping drops and the screen parameter. The typical dripping drops are ranging from 3.5 mm to about 6 mm in our studies.

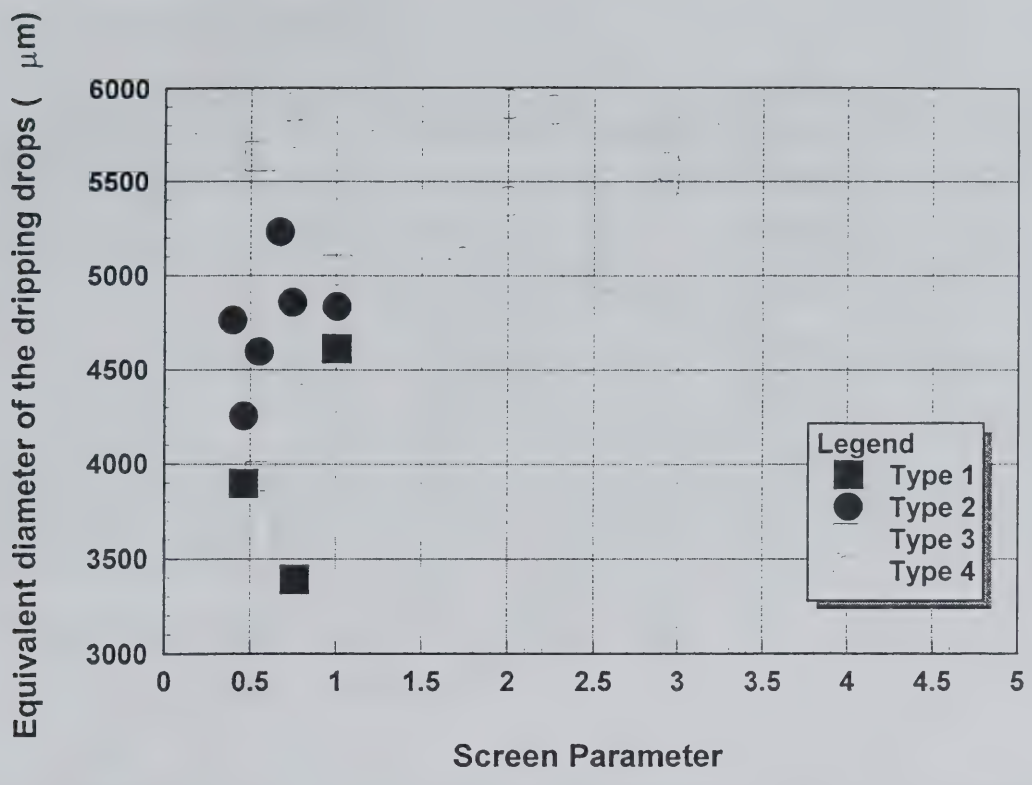

Figure 5.7 Size measurement of the dripping drops from horizontal screens

Smaller dripping drops are associated with coarser screens. In general, if the width of the mesh opening is wide enough so that only dripping drops from the wires are encountered, the dripping size decreases as the wire size decreases.

Hung (1998) derived a correlation of the dripping drop size as a function of single wire diameter. This Equation (4.8) is restated here to quantify the size of the dripping drop:

$$D' = 1.813D\left(\frac{D}{\sqrt{\sigma/\rho_L g}}\right)^{-0.786} \qquad (4.8)$$

Figure 5.8 shows the comparison between the prediction of drops dripping from single wires and the dripping drops from the screens in Type 1 situation. If the screens are coarse enough such that the dripping drops are formed at the bottom side of the wires, then the above expression can be used to predict the dripping drop size reliably.

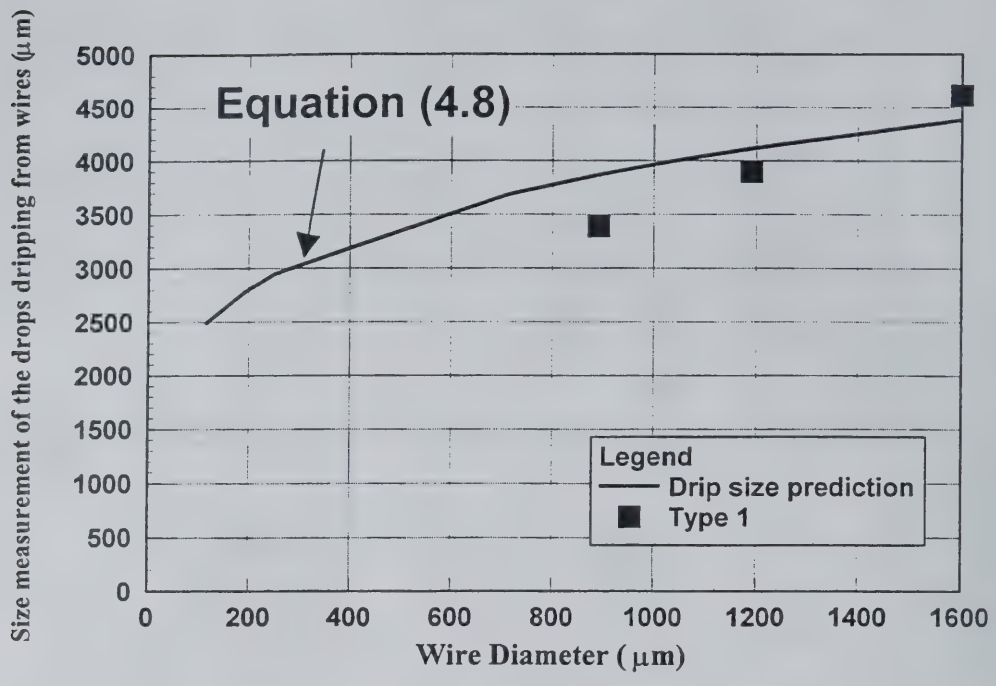

Figure 5.8 Plot of size of dripping drops from the underside of wires on a screen verses prediction from single wires situation

From our results displayed in Figure 5.8, the largest dripping drops are formed from the fine screen situations which resemble the flat plate dripping situation. Tamada and Shiback (1966) derived an expression for a drop slowly formed by dripping from a horizontal flat surface, based on a balance between the gravitational and the surface tension forces, as follows:

$$D' = 3.3\left(\frac{\sigma}{\rho_L g}\right)^{0.5} \qquad (5.2)$$

Therefore, for a water drop dripping off from a flat surface at a very slow flow rate, its diameter would be about 9 mm. It is worth to note that even though a very fine screen may look like a solid flat surface with similar dripping observation, the dripping mechanisms in both cases are quite different. Therefore, equation (5.2) may be used to provide the maximum diameter limit of a water dripping drop.

5.6 Concluding Remarks

An investigation of the water droplets impacting on wire mesh screens was studied experimentally. Experimental results showed that some droplets might pass through the screen without hitting it. For the droplets which impacted on the screen directly, the dominant outcome of the impaction was dripping. The dripping characteristics depended on the incoming droplet velocity, the wire diameter of the screen, and the size of the mesh opening. For droplets impacting on coarse screens, the dripping phenomena resembled the situations for single wire. For droplet impacting on fine screens, a thin water film was formed on the top of the screen and it gradually permeated to the bottom side through the small mesh openings. This film continued to grow underneath in a form of a pendant drop under the gravity effect. Eventually when the weight of the pendant drop was large enough to overcame the surface tension effect associated with the contact surface of the screen, the drop detached from the screen and dripped off. Non-dimensional parameters could be used to analyze the outcome of the impaction characteristics.

Chapter Six

Summary and Recommendations

6.1 Summary of the Research

The present research has been carefully designed to examine the key fundamentals of the transport mechanisms, impaction, and penetration of water mist droplets, and to predict their implications through compartment openings during fire situations. Particularly, the transport and the impacting dynamics of spray droplets on objects with complex geometry have been investigated. The two-phase gas droplet transport in the vicinity of a variety of objects was examined numerically using the computational fluid dynamics framework. The collection and penetration characteristics of droplets through an array of objects were modeled and formulated analytically. The impacting dynamics of droplets on wires and screens were also investigated experimentally. The general conclusions of this research accomplished are outlined below:

The analysis of the droplets falling in stagnant air shows that the volumetric spectrum has a high population of the smaller droplets. In addition, there is a considerable time delay of the arrival of the mist sprays than that of the typical sprinkler drops.

Numerical CFD modeling to investigate the transport of droplets in a gaseous surrounding around the objects with complex geometry was successful in visualizing the droplet distributions in the vigorous flow field. An analysis based on the two-phase Navier-Stokes equations was achieved to reveal the motions of droplets in the vicinity of rectangular strips at an isothermal environment. When Re is about 3125, a transient vortex shedding was found behind the strip. Small droplets (<50 μm) would follow the air streams of the flow wake in order to migrate to the center area beneath the strip and probably to reach the fire. This illustrates that water mist has a better chance to reach the fire behind the obstructions.

The non-dimensional impaction parameter (K) was determined to be a good parameter to determine the deposition patterns on the surface of a single or multiple objects. The penetration efficiency of droplets through an array of objects was formulated using the collection efficiency (η) and geometry consideration (B). It was recommended that the penetration efficiency of a 3-D complex screen object could be approximated by using the results of the 2-D rectangular strip through equation (2.11) with reasonable agreement.

The impacting dynamics of the droplets onto the opening structures of the equipment compartment has also been investigated parametrically by considering the droplets impaction on wires and screens. The effect of droplet velocity, droplet sizes, wire sizes, and wire mesh configurations were varied parametrically to reveal the impaction characteristics. Both the droplet stream and drop-on-demand generators were feasible to produce the droplets in a wide variety of operating conditions for the impaction studies.

The typical modes of impaction outcome on wires were disintegration and dripping. Drop disintegration was likely to occur if the incoming droplets with high velocity impacted on the wires with smaller diameter. On the other hand, larger dripping drops were formed if the droplet velocity was low or the wire diameter was large. A non-dimensional map was obtained to identify the regime of disintegration mode, the momentum induced dripping mode, and the gravity induced dripping mode. This map could be used to predict the impacting outcome at similar conditions.

The size of the dripping drops increased with increasing wire diameter. The non-dimensional dripping size had also been correlated well with the Bond number. A linear trend on a log-log plot exhibited that the Bond number was an important parameter for dripping drop size measurement. In addition, the contact angle effect was also examined by studying the droplets impacting on waxed wire. The drops dripping from waxed wires were generally smaller than the ones from the non-waxed wires due to the reduced surface tension effect at the interfacial contact.

Another investigation of the water droplets impacting on wire mesh screens was also studied experimentally. Experimental results showed that some droplets would pass through the screen without hitting it. For the droplets which impacted on the screen directly, the dominant outcome of the impaction was dripping. The dripping characteristics were dependent upon the incoming droplet velocity, the wire diameter of the screen, and the size of the mesh opening. For droplets impacting on coarse screens, the dripping phenomena resembled the situations for single wire. For droplet impacting on fine screens, a thin water film was formed on the top of the screen and it gradually permeated to the bottom side through the small mesh openings. This film continued to grow underneath in a form of a pendant drop under the gravity effect. Eventually when the weight of the pendant drop was large enough to overcome the surface tension effect associated with the contact surface of the screen, the drop detached from the screen and drips off. Non-dimensional Screen parameter was found to be a good way to correlate with the size of the large dripping drops.

This research has provided a promising procedure to systematically evaluate the dynamics, impaction, and penetration of droplets through the complex objects. For example, in applying a water mist for suppressing fire inside an equipment compartment, it is desired to determine the behavior and the subsequent condition of the mist droplets while they are penetrating into the compartment. Therefore, if the initial mist and gas conditions (droplet size, drop impacting velocity, gas velocity, and so on) and the configurations of the complex objects (dimension of structure, blockage to opening ratio, etc.) are given, the amount of mist penetrating through the openings of the objects can be predicted based on the number densities, inertial impaction parameter, and penetration efficiency (equation 2.11) through the flow analysis. The droplets which penetrate through directly will likely be governed by the gas streams. Then, for those droplets intercepted by the structure, non-dimensional regime maps and correlations developed in this study can be employed to predict their impacting behavior and outcome subsequent to the impaction processes.

6.2 Recommendations of Areas for Future Research

A few areas for future research have been identified in continuation of the work already accomplished in the present report. They are listed as follows:

- The analysis of the droplet transport using the computational fluid dynamics approach has been demonstrated to be reasonably successful in understanding the complex flow interactions between the turbulent gas streams, droplet dynamics, and the geometry of the objects. However, this investigation concentrates mainly on the dynamics and transport of droplets in an isothermal environment, in which there is no droplet evaporation being considered. In many other situations, for example, in the presence of a temperature field, there exists high temperature gradient regions in the flow field and the mists may evaporate and become vapor rapidly. The effect of mist evaporation may become important for the effectiveness of water mists in fire suppression. Therefore, taking into the effect of droplet evaporation into account may yield more meaningful results, particularly for the purpose of understanding water mist transport for fire suppression.

- In accordance with the above recommendation, for the droplet impaction experiments accomplished, the wires and the screens were at the ambient temperature. It may be of practical interest to continue the droplet impaction on heated wires and screens to reveal the effect of temperature into the overall picture of analysis. Other objects such as strips or rods could also be examined for the impaction study.

References

Amsden, A.A., O'Rourke, P.J., and Butler, T.D., 1985, "A Computer Program for Chemically Reactive Flows with Sprays," Los Alamos Scientific Laboratory Report, LA-9069-T.

Ashgrizzadeh, N., and Yao, S.C., 1983, "Development of Multi-orifice Impulsed Spray Generators for Heterogeneous Combustion Experiments" *ASME/JSME Thermal Engng. Joint Conf. Proc.* Vol.2, pp. 429-433.

Beckwith, T.G., and Parangoni, R.D., 1990, *Mechanical Measurements, 4th ed.*, Addison-Wesley, Reading, Massachusetts, pp. 346-348.

Bussmann, M., Chandra, S. & Mostaghimi, J., 1997, "Droplet Impact onto Arbitrary Surface Geometries," In *Proc. ASME Fluids Engineering*, FEDSM97-3073.

Capps, R.W., 1994 "Properly specify wire-mesh mist eliminators," *Chem. Eng. Progress*, Vol. 90, n 12, pp. 49-55.

Cazabat, A., 1987, "How does a droplet spread?" *Contemp. Phys*, **28,** pp.347-364.

Chandra S., and Avedisian, C.T., 1991, "On the collision of a droplet with a solid surface," *Proc. R. Soc. Lond., A* **432,** pp.13-41.

Cheng, Y.S., and Yeh, H.C., 1980, "Theory of a screen-type diffusion battery," *J. Aerosol Sci.*, Vol. 11, pp. 313-320.

Chow, C.Y., 1979, *An Introduction to Computational Fluid Mechanics*, John Wiley & Sons, New York.

Chung, T.J., 1993, *Numerical Modeling in Combustion*, Taylor & Francis, Washington, DC.

Cohen, R.D., 1991, "Shattering of a liquid drop due to impact," *Proc. R. Soc. Lond. A* , **435,** pp. 483-503.

Dear, J.P., and Field, J.E., 1988, "High-speed photography of surface geometry effects in liquid/solid impact," *J. Appl. Phys.,* **63**, pp. 1015-1021.

Eleftheriadis, K., and Colbeck, I., 1992, "The Particle Collection Efficiency of Rectangular Strips by Inertial Impaction," *J. Aerosol Sci.,* Vol. 23, Suppl. 1, pp. S35-S38.

Feord, D., Wilcock, E., and Davies, G.A., 1993, "A stochastic model to describe the operation of knitted mesh mist eliminators, computation of separation efficiency," *Trans. IChemE*, Vol. 71, part A, pp. 282-294.

Fukai, J., Shiiba, Y., Yamamoto, T., Miyatake, O., Poulikakos, D., Megaridis, C.M., and Zhao, Z., 1995, "Wetting effects on the spreading of a liquid droplet colliding with a flat surface: Experiment and Modeling," *Phys. Fluids*, 7 (2) pp. 236-247.

Golovin, M. N., and Putman, A. A., 1962, "Inertial Impaction on Single Elements," *Ind. Eng. Chem. Fundamentals,* Vol. 1, No. 4, pp. 264-273.

Hahner, F., Dau, G., and Ebert, F., 1994, "Inertial impaction of aerosol particles on single and multiple spherical targets," *Chemical Engineering & Technology,* Vol. 17, n 2, pp. 88-94.

Harlow, F.H., and Shannon, J.P., 1967, "The Splash of a Liquid Drop," *J. Applied Phys.*, Vol. 38, No. 10, pp. 3855-3866.

Hung, L.S., 1998, "Investigations of the Transport and Dynamics of Droplets Impacting on Complex Objects," Ph.D. Thesis, Carnegie Mellon University, Pittsburgh, PA.

Hung, L.S., and Yao, S.C., 1998, "Experimental studies of water droplets impacting on cylindrical wires," Paper No. 660, *Proc. of 1998 3rd International Conf. of Multiphase Flow*, Lyon, France.

Hung, L.S., and Yao, S.C., 1998, "An Experimental Study of Droplets Impacting on Screens," Accepted for presentation at the Characterization of Flow Patterns in Multiphase Flow Systems Session of the 1998 *ASME International Mechanical Engineering Congress and Exhibition*, Anaheim, CA.

Hung, L.S., and Yao, S.C., 1997, "Investigations on the Phenomena of Water Droplets Impacting on Cylindrical Objects," Submitted, *International Journal of Multiphase Flow.*

Hung, L.S., and Yao, S.C., 1997, "Study of droplet impaction on wires for fire suppression applications," *Proc. of ASME National Heat Transfer Conference*, HTD-341, Vol.3, pp.13-18.

Hung, L.S., and Yao, S.C., 1997, "Numerical Studies on the Transportation of Water Mist for Fire Suppression Applications," *Proceedings of the ASME Heat Transfer Division*, HTD-352, Vol. 2, pp. 73-80.

Hung, L.S., and Yao, S.C., 1997, "Evaluation of Water Mist Penetration Through Complex Openings of Compartments," Presented at the 1997 *2nd International Conference on Fire Research and Engineering,* Gaithersburg, Maryland.

Hung, L.S., and Yao, S.C., 1997, "Interactions of Droplets with Cylindrical Objects," Presented at the 1997 *ILASS-Americas, 10th Annual Conference of Liquid Atomization and Spray Systems*, Ottawa, Ontario, Canada.

Hung, L.S., and Yao, S.C., 1996a, "Experimental Investigation of the Water Mist Impacting Phenomenon on Horizontal Wires," Presented at *Annual Conference on Fire Research*, Gaithersburg, Maryland.

Hung, L.S., and Yao, S.C., 1996b, "Numerical Studies on the Deposition and Transport of Water Mist to a Horizontal Plate," Presented at *Annual Conference on Fire Research*, Gaithersburg, Maryland.

Ichitsubo, H., Hashimoto, T., Alonso, M., and Kousaka, Y., 1996, "Penetration of ultrafine particles and ion clusters through wire screens," *Aerosol Science and Technology*, Vol. 24, n 3, pp. 119-127.

Ilias, S., and Douglas, P.L., 1989, "Inertial Impaction of Aerosol Particles on Cylinders at Immediate and high Reynolds Numbers," *Chem. Eng. Sci.*, Vol. 44, No. 1, pp. 81-99.

Jones, A., and Nolan, P.F., 1995, "Discussions on the use of fine water sprays or mists for fire suppression," *J. Loss. Prev. Process Ind.*, Vol. 8, No. 1, pp. 17-22.

Konstandopoulos, A., Labowsky, M.J., and Rosner, D.E., 1993, "Inertial deposition of particles from potential flows past cylinder arrays," *J. Aerosol Sci.*, Vol. 24, n 4, pp. 471-483.

Karl, A., Anders, K. & Frohn, 1994, "A. Experimental Investigation of Droplet Deformation During Wall Collisions by Image Analysis," In *Proc. of ASME Winter Annual Meeting*, FED-Vol. 172, pp. 135-141.

Langmuir, I., and Blodgett, K.B., 1946, U.S. Army Air Force Tech Report. No. 5418.

Lefebvre, A.H., 1989, *Atomization and Sprays*, Hemisphere Publishing Co., London.

Lesser, M.B.,1981, "Analytic Solutions of liquid-drop impact problems," *Proc. R. Soc. Lond. A*, **377**, pp. 289-308.

Levin, A. & Hobbs, P.V., 1971, "Splashing of water drops on solid and wetted surfaces: Hydrodynamics and charge separation," *Phil. Trans, R. Soc. London A*, **269**, pp. 555-585.

Lindblad, N.R., and Schneider, J.M., 1965, "Production of uniform-sized liquid droplets," *J. Sci. Instrum.*, **(42)**, pp. 635-638.

Liu, H., Lavernia, E.J. & Rangel, R.H., 1994, "Modeling of molten droplet impingement on a non-flat surface," In *Proc. of ASME Fluid Engineering*, FED- Vol.201, pp. 1-5.

May, K.R., and Clifford, R., 1967, "The Impaction of Aerosol Particles on Cylinders, Spheres, Ribbons, and Discs," *Ann. Occup. Hyg.*, No. 10, pp. 83-95.

Muldoon, J., 1984, "Screens and screening," *Chem Eng (New York),* Vol. 91, n3, pp. 90-94.

Noll, K. E., and Pilat, M. J., 1970, "Inertial Impaction of Particles upon Rectangular Bodies," *J. Colloid & Interface Sci,* Vol. 33, No. 2, pp.197-207.

Ramsen, N., 1996, "Water Mist - a Status Update," *J. Fire Prev.*, Vol. 287, pp.16-20.

Ranz, W.E., and Wong, J.B., 1952, "Impaction of Dust and Smoke Particles," *Ind. Engng. Chem.,* Vol. 44, No. 6, pp.1371-1381.

Rayleigh, L., 1879, "On the Stability of Jets," *Proc. Lond. Math. Soc.,* **10**, pp. 4-13.

Rein, M., 1993, "Phenomena of liquid drop impact on solid and liquid surfaces," *Fluid Dynamics Research*, **12**, pp. 61-93.

Savart, F., 1833, *Ann. Chim. Phys.*, **(53)**, pp. 337-386.

Schneider, J.M., 1964, *Ph.D. Dissertation*, University of Illinois.

Schneider, J.M., and Hendricks, C.D., 1964, "Source of Uniform-Sized Liquid Droplets," *Rev. Sci. Instrum., 35,* **(10)**, pp. 1349-1350.

Soar, R.K.H., 1991, "Woven wirecloth - historical development and modern methods," *Wire Industry*, Vol. 58, No. 688, pp. 197-199.

Shang, H., 1992, "Numerical Studies of Spray Combustion In Liquid-Fueled Engines," Ph.D. Thesis, University of Alabama.

Tamada and Shiback, 1966, cited in Atomization - a survey and Critique of the Literature, by C.E. Lapple, J.P. Henry, and D.E. Blake, Stanford Research Institute report No. 6.

Wang, H.C., 1996, "Comparison of thermal rebound theory with penetration measurements of nanometer particles through wire screens," *Aerosol Science and Technology,* Vol. 24, n 3, pp. 129-134.

Yang, J.C., 1996, Private Communication, NIST.

Yao, S.C., and Cai, K.Y., 1988, "The Dynamics and Leidenfrost Temperature of Drops Impacting on a Hot Surface at Small Angles," *Experimental Thermal and Fluid Science*, **1,** pp. 363-371.

Yao, S.C., Hochreiter, L.E., and Cai, K.Y., 1988, "Dynamics of Droplets Impacting on Thin Heated Strips," *J. Heat Transfer*, **110,** pp. 214-220.

Zhao, Z., Poulikakos, D., and Fukai, J., 1996a, "Heat transfer and fluid dynamics during the collision of a liquid droplet on a substrate - I. Modeling.," *Int. J. Heat Mass Transfer* **39**, pp. 2771-2789.

Zhao, Z., Poulikakos, D., and Fukai, J., 1996b, "Heat transfer and fluid dynamics during the collision of a liquid droplet on a substrate - II. Experiments.," *Int. J. Heat Mass Transfer* **39**, pp. 2791-2802.

NIST-114 (REV. 6-93) ADMAN 4.09

U.S. DEPARTMENT OF COMMERCE
NATIONAL INSTITUTE OF STANDARDS AND TECHNOLOGY

MANUSCRIPT REVIEW AND APPROVAL

(ERB USE ONLY)	
ERB CONTROL NUMBER: G	DIVISION:
PUBLICATIONS REPORT NUMBER: No.	CATEGORY CODE:
PUBLICATION DATE:	NO. PRINTED PAGES:

INSTRUCTIONS: ATTACH ORIGINAL OF THIS FORM TO ONE (1) COPY OF MANUSCRIPT AND SEND TO: WERB SECRETARY, BUILDING 820, ROOM 125

TITLE AND SUBTITLE (CITE IN FULL)

Investigation of Droplet Penetrations through Complex Openings of Compartments

CONTRACT OR GRANT NUMBER: 60NANB5D0093

TYPE OF REPORT AND/OR PERIOD COVERED: NIST-GCR-98-759

AUTHOR(S) (LAST NAME, FIRST INITIAL, SECOND INITIAL)
Yao, S.C. and Hung, L.S.

PERFORMING ORGANIZATION (CHECK (X) ONE BOX)
- [X] NIST/GAITHERSBURG
- [ ] NIST/BOULDER
- [ ] NIST/JILA

LABORATORY AND DIVISION NAMES (FIRST NIST AUTHOR ONLY)

SPONSORING ORGANIZATION NAME AND COMPLETE ADDRESS (STREET, CITY, STATE, ZIP)
Department of Mechanical Engineering, Carnegie Mellon University, Pittsburgh, PA 15213

PROPOSED FOR NIST PUBLICATION

[ ] JOURNAL OF RESEARCH (NIST JRES)	[ ] MONOGRAPH (NIST MN)	[ ] LETTER CIRCULAR
[ ] J. PHYS. & CHEM. REF. DATA (JPCRD)	[ ] NATL. STD. REF. DATA SERIES (NIST NSRDS)	[ ] BUILDING SCI. SERIES
[ ] HANDBOOK (NIST HB)	[ ] FEDERAL INFO. PROCESS. STDS. (NIST FIPS)	[ ] PRODUCT STANDARDS
[ ] SPECIAL PUBLICATION (NIST SP)	[ ] LIST OF PUBLICATIONS (NIST LP)	[ ] OTHER
[ ] TECHNICAL NOTE (TN)	[ ] INTERAGENCY/INTERNAL REPORT (NISTIR)	[ ] —

PROPOSED FOR NON-NIST PUBLICATION (CITE FULLY): [ ] —U.S. FOREIGN— [ ]

PUBLISHING MEDIUM:		PAPER		DISKETTE		CD-ROM		WWW		OTHER

SUPPLEMENTARY NOTES

ABSTRACT (A 2000-CHARACTER OR LESS FACTUAL SUMMARY OF MOST SIGNIFICANT INFORMATION. IF DOCUMENT INCLUDES A SIGNIFICANT BIBLIOGRAPHY OR LITERATURE SURVEY, CITE IT HERE. SPELL OUT ACRONYMS ON FIRST REFERENCE.) (CONTINUE ON SEPARATE PAGE, IF NECESSARY.)

The use of fine water mist as one of the possible Halon 1301 replacements has been identified for certain fire suppression situations in equipment compartments. One current research effort is to apply the water mist sprays to suppress the fire occurring in hidden locations behind obstructions or inside the equipment compartments.

Since the mist usually contains a spectrum of drop sizes, the smaller mist droplets may follow the gas streams closely and penetrate directly through the slots of the obstructions while the larger droplets may be intercepted or impacted by the obstructions. When the mist droplets are approaching the structures, the overall penetrating process of the mist flow through the obstruction depends strongly on the transport of the mist droplets in the gas streams, the ability of the droplets flowing through the obstruction, and the behavior of droplets subsequent to the impaction.

The present research presents an integrated approach to model the penetration of water mist through the obstruction for fire suppression applications. Firstly, numerical investigations employing the two-phase Navier-Stokes equations are achieved by using computational fluid dynamics (CFD) to evaluate the overall transport of droplets in the vicinity of the openings, which include rectangular strips and a 3-D screen object. In particular, the motions of the droplets coupled with the gas flow field around the objects are analyzed. The deposition of droplets on the objects and their penetration through the spacing of the objects are also formulated. Then, experimental investigations are performed to address the actual impacting phenomena of droplets on objects. Droplet generators are designed to generate droplets in a variety of operating conditions. Structures such as cylindrical wires and mesh screens are examined in the impaction experiments. Images of the impacting phenomena are analyzed through digital image processing. Non-dimensional regime maps and the correlations of the impaction outcome are also developed. The conclusions from both the numerical and experimental investigations are integrated to provide an overall understanding to the complex interaction phenomena and to establish a procedure for predicting the outcome of similar processes.

KEY WORDS (MAXIMUM OF 9; 28 CHARACTERS AND SPACES EACH; SEPARATE WITH SEMICOLONS; ALPHABETIC ORDER; CAPITALIZE ONLY PROPER NAMES)
CFD models; compartments; droplets; fire suppression; penetration; water mist

AVAILABILITY:
- [X] UNLIMITED
- [ ] FOR OFFICIAL DISTRIBUTION - DO NOT RELEASE TO NTIS
- [ ] ORDER FROM SUPERINTENDENT OF DOCUMENTS, U.S. GPO, WASHINGTON, DC 20402
- [ ] ORDER FROM NTIS, SPRINGFIELD, VA 22161

NOTE TO AUTHOR(S): IF YOU DO NOT WISH THIS MANUSCRIPT ANNOUNCED BEFORE PUBLICATION, PLEASE CHECK HERE. [ ]